UNIVERSITY OF OKLAHOMA

GRADUATE COLLEGE

ORGANIC-RICH SHALE TENSILE STRENGTH MODELING

A THESIS

SUBMITTED TO THE GRADUATE FACULTY

in partial fulfillment of the requirements for the

Degree of

MASTER OF SCIENCE

By

THAO PHUONG LE
Norman, Oklahoma
2016

ORGANIC-RICH SHALE TENSILE STRENGTH MODELING

A THESIS APPROVED FOR THE
CONOCOPHILLIPS SCHOOL OF GEOLOGY AND GEOPHYSICS

BY

_____
Dr. Younane Abousleiman, Chair

_____
Dr. Roger Slatt

_____
Dr. Ahmad Ghassemi

ACKNOWLEDGEMENTS

I would like to express my wholehearted appreciation to my advisor, Dr. Younane Abousleiman, for his silent encouragement and patient guidance. I thank him for giving me the opportunity to work with him, beginning as an undergraduate at iPMI. For more than three years, I have learned to become emotionally and physically stronger. I sincerely appreciate him for teaching me to be an independent researcher and scientist. Without his guidance, the completion of this thesis would be impossible.

I also would like to thank both of my committee members, Dr. Roger Slatt and Dr. Ahmad Ghassemi, for their valuable time and for sharing with me their expertise in this work. My deep appreciation also goes to Ms. Carla Cates. I would never forget her caring support whenever I stopped by her office. As a young woman living far away from home, I felt like I could share my feelings with her and she helped me get over the toughest time of graduate study. I am also thankful to my colleagues at iPMI, Dr. Son Hoang, Dr. Minh Tran, Mr. Chao Liu, for their contribution to the valuable discussions and feedback on my work. My special thanks also extends to my office mates, Junxin Guo and Batoul Maatouk, for academic discussions, humor and jokes; to my best friends, Duc Nguyen, Trung Nguyen, and Tham Nguyen, for all the wonderful moments and thoughts we shared through all these years. Thank you for keeping me smiling all days and delivering this work to reality.

Most importantly, I cannot express enough words to thank my family for their unconditional love and support that makes me strong, yet beautiful, through my whole life.

TABLE OF CONTENTS

LIST OF TABLES

LIST OF FIGURES

ABSTRACT

Shale mechanical characterization is an expensive and time intensive lab and field exercise. Experimental observations in lab shale characterization have shown some relation (linear or non-linear) between fracture toughness and tensile strength. Both fracture toughness and tensile strength measurements require a lot of laboratory work, yet porosity and mineralogy estimation can be quickly and easily obtained using conventional logging tools. In this study, attempts were taken to predict fracture toughness and tensile strength as a power function of clay and non-clay phase porosity and correlate this to the shale matrix organic content. The model was then expanded to relate to Mode-I fracture toughness of shale as well. It was also verified by experimental results of the same data set of Woodford shale in this work.

Using the data set of Woodford shale, the correlations between lateral tensile strength, T_p, with non-clay mineral content, clay content, TOC, and porosity were observed. It was suggested that all of these individual components might add up to a single, yet more representative, parameter called clay packing density or alternatively, clay phase porosity. This property describes how tightly the clay particles are packed together in the shale mineral matrix. Combining this knowledge with previously published micromechanics studies in upscaling strength of porous poly-crystals from porosity, it was hypothesized that tensile strength for many kinds of shale might also act as a function of porosity. However, as the clay minerals phase plays a significant role in shale tensile failure, porosity of clay phase (i.e., clay phase porosity) was selected as the fundamental input for this model. Particularly, using mineralogical information and conventional porosity measurements, clay phase porosity for many kinds of shale

including Woodford shale, Eagle Ford shale, Hydro shale, Mancos shale, Barnett shale, Dotternhausen (Posidonia) shale, and Wickensen (Posidonia) shale was computed as primary input for the model of shale tensile strength.

For organic-free shale, the model proves that the granular nature of clays and non-clay minerals primarily controls tensile strength of these rocks. The fact that the model shows a well-defined decreasing trend in tensile strength as clay phase porosity increases, means that the model is flexible to be applied for many kinds of shale, regardless of their mineralogical composition and porosity or multi-porosity nature. On the other hand, for organic-rich shale, the kerogen content was incorporated into the model by modifying the original calculation of clay phase porosity of kerogen-free shale. A decreasing trend in tensile strength was also observed as this modified clay phase porosity increases. To some extent, given that the model only needs mineralogy information, kerogen content, and porosity as primary input for tensile strength estimation, it almost fulfills the hope to simplify the polymer nature of kerogen observed in organic-rich shale yet absent in organic-free shale. However, it was discovered that the modulus of toughness of kerogen-bearing shale, defined as the work/energy needed before the total rupture, is significantly higher (~10x) than that of kerogen-free shale. As a result, the kerogen effect on the modulus of toughness and or the tensile strength is much larger than the anisotropy effect ever observed in classical tensile strength testing protocols. For that reason, mineralogy information and porosity are only enough to quantify the granular nature, but not the polymer woven into the clay and non-clay matrices behavior as was recently observed in kerogen-rich shale experiments. It was suggested that this model as well as other existing models using

empirical equations to predict tensile strength of organic-rich shale might not be perfect to be a composite model for KRS in general. As a result, refinements are indeed necessary.

CHAPTER 1: INTRODUCTION

1.1 Motivation

In recent years, knowledge of shale depositional and diagenetic processes and how they affect shale mechanical and physical properties has been applied extensively in unconventional reservoir characterization. The role of the multi-mineral structure and composition on the mechanical properties has been identified for shale (Ulm and Abousleiman 2006; Abousleiman et al. 2007; Abousleiman et al. 2009; Sierra et al. 2010). Unconventional reservoir shale has long been known by its characteristic content of organic matter and, in particular, large content of kerogen (Sierra et al. 2010; Slatt and Abousleiman 2011). For more than a decade, organic-rich shale has been the subject of micro- and nano-mechanical characterization as a result of advances in nanotechnology. Early nanoindentation studies on shale and mudstones were conducted on shale samples that contained only "traces" of organic matter, which means the organic matter had little effect on the overall mechanical behavior. Zeszotarski et al. (2004) progressed the nanoindentation study of shale by relating kerogen stiffness and anisotropy to the maturity of the organic-rich Woodford shale. However, the tested samples in this study were in unsaturated conditions, which means the results do not fully represent shale at *in-situ* conditions. After that, a series of extensive nanoindentation studies conducted on Woodford shale allowed for the observation of kerogen effect on the overall mechanical response of organic-rich shale (Abousleiman et al. 2007; Ortega et al. 2007; Abousleiman et al. 2009). It was concluded that the higher percent volume of kerogen in Woodford shale decreased the degree of anisotropy of its mechanical parameters (Ortega et al. 2009).

Abousleiman et al. (2016) in their recent publication have illustrated the contribution of kerogen to shale mechanical tensile strength. Earlier works have addressed the effects of kerogen on the mechanical characterization and the elastic and geophysical properties of organic-rich shale and organic-free shale (Vernik and Nur 1992; Ortega et al. 2009). Abousleiman et al. (2016) then describe how the polymer nature of kerogen and its spatial distribution within the shale mineral matrix affect the mechanical behavior of organic-rich shale. It was found that kerogen, in the tensile loading configuration, acts like a cross-linked polymer with significant tensile strength and a very large tensile modulus of rupture, as compared to the brittle behavior of granular shale matrix minerals (Abousleiman et al. 2016).

Given that the study by Abousleiman et al. (2016) sheds new light on the composite nature of organic-rich shale tensile failure, available research in the literature on strength properties of organic-rich shale under tensile loading configuration (such as hydraulic fracturing) is still very limited. Moreover, strength properties of shale formations are usually obtained through laboratory analyses. The required core samples are often expensive and not always in the best condition (i.e., damaged from core retrieval process). Due to the fissile nature and the chemical reactivity of shale, core preservation and sample preparation require extra care and effort before doing any measurements. As a result, the scope of this study is to provide a model to predict ultimate indirect tensile strength and Mode-I fracture toughness for many kinds of organic-rich shale such as Woodford shale, Eagle Ford shale, Barnett shale, etc., using parameters that can be easily obtained using conventional logging tools and provided along with appropriate calibrations from laboratory measurements.

1.2 Importance of Indirect Tensile Strength and Fracture Toughness

Rock mechanics engineers are less concerned with obtaining the tensile or fracture strength of a brittle rock at low mean stresses. Because of the jointing and faulting that creates the inherent discontinuities in the rock mass, tensile strength is usually taken to be negligible (Ratigan 1982). Despite the fact that tensile strength of brittle rock is often ignored, there are a number of applications in rock mechanics wherein the knowledge of tensile strength is of fundamental importance. The apparent tensile strength is, indeed, necessary in a hydraulic fracture experiment that determines *in-situ* stress condition; particularly for the state of stress that results from the initiation of a hydraulically-induced fracture (Ratigan 1982).

The mechanics of the fracture process in shale is clearly important from an engineering standpoint. To maximize the efficiency of hydraulic fracturing, shale characterization is necessary and requires knowledge of many fundamental parameters such as mineralogy, TOC, thermal maturity, porosity, permeability, fracture density and orientation, static and dynamic geomechanical properties (Young's modulus, Poisson's ratio), uniaxial and triaxial compressive strength, internal friction angle, cohesion, Biot's coefficient, tensile strength, fracture toughness, brittleness, etc. (Abousleiman et al. 2007; Abousleiman et al. 2009; Slatt and Abousleiman 2011; Sierra 2011). Some parameters can be easily obtained using logging tools, but others require time and effort to obtain reliable laboratory measurements. Rock specimens for laboratory measurements ideally should be obtained from retrieved cores from the subsurface. Fracture toughness testing is expensive and time-consuming. Therefore, it is impractical to measure fracture toughness of the entire well section by conventional methods. That,

in turn, leads to the importance of developing a convenient method to measure and estimate fracture toughness.

Many studies have been focused on establishing an empirical relationship between fracture toughness and other popular and easily obtained mechanical parameters of rock. Brown and Reddish (1997), Al-Shayea et al. (2000), and Nasseri and Mohanty (2008) have conducted many experiments to derive an approximation of fracture toughness from many other parameters, such as hardness index, tensile strength, uniaxial compressive strength, elastic modulus, Poisson's ratio and density, etc. Using the complete laboratory data set of Woodford shale from the study by Sierra et al. (2010), an attempt was made to verify some simple correlations relating Mode-I fracture toughness with Young's modulus, compressional wave velocity, tensile strength, and density. Among these four correlations, a highly reliable relationship exists between Mode-I fracture toughness and tensile strength in Woodford shale (R^2=0.93). As a result, this relation definitely possesses a positive potential; i.e., if we are able to predict tensile strength from common and easily obtained parameters, Mode-I fracture toughness can be estimated as well.

1.3 Thesis Outline

This chapter (Chapter I: Introduction) includes the motivation behind selection of this thesis topic, the importance of indirect tensile strength and fracture toughness to this study, and an outline for the thesis. Chapter 2 contains a brief literature review of fracture toughness and tensile strength. Some major questions to be addressed include:

- Which correlations are available to estimate fracture toughness? How do they differ from each other? Why are such derivations useful to the petroleum industry?
- Which mechanical factors and geometrical aspects control tensile strength of organic-rich shale? Is it the kerogen or the mineral matrix of the shale or both?

By addressing these questions and reviewing insights from the literature on the granular and polymer nature of kerogen-rich shale, the puzzle pieces are collected and are the foundation for the modelling work. Based on the spatial distributions and interactions between non-clay minerals, clay minerals, kerogen, and pores in organic-rich shale, Chapter 3 explains how the tensile strength modeling was approached and conducted. The dominant role of clay minerals was recognized through a parameter called clay phase porosity in controlling shale tensile strength. By including kerogen content into the original calculation of clay phase porosity in kerogen-free shale, a potential power relation was observed between tensile strength and the new clay phase porosity for many kinds of organic-rich shale, such as Woodford shale, Eagle Ford shale, Barnett shale, etc.

Chapter 4 expands on preliminary results outlined in Chapter 3. Modification of the model by new data of compacted clay and sand was then introduced to better include percolation threshold of clay phase porosity at 50%. From here, the upper and lower bounds of the models are also established by ultimate tensile strengths of hydroxyapatite and gypsum single crystal, respectively, to constrain the possible range of ultimate tensile strength of homogeneous ‘single crystal’ of shale. Next, using the linear relationship between Mode-I fracture toughness and tensile strength reported

from many previous experimental studies, the model is extrapolated to derive a power function to estimate fracture toughness from clay phase porosity. Measured fracture toughness of Woodford shale samples shows promising results using this model. Last but not least, discussion on the effect of kerogen in the granular and polymer of kerogen-rich shale explains why this model has simplified the tensile behavior of a complex “composite polymer-type weaved porous material”. That says future improvements in studying this composite material is indeed necessary.

CHAPTER 2: LITERATURE REVIEW - COLLECTING EVIDENCE

2.1 Hydraulic Fracturing and What is Behind the Griffith's Criterion

Hydraulic fracturing has been a popular topic in both industry and academia since the boom of oil and gas exploration in unconventional shale. Such stimulations via hydraulic fracturing dictate mixed-mode (opening and sliding modes) fracture initiation. Figure 2.1.1 shows three modes of crack surface displacement: opening mode, sliding mode, and tearing mode. Fractures of Mode I and II are the two primary types in hydraulic fracturing (Backers 2005). Opening mode contributes to fracture opening, and sliding mode contributes to fracture reorientation from the preexisting fracture.

- Mode I is a tensile-mode crack, where the crack surfaces move directly apart. This allows the crack to propagate in its own plane.
- Mode II is a shear-mode crack (sliding), where the crack surfaces slide over one another in a direction perpendicular to the leading edge of the crack. This sort of crack cannot propagate in its own plane.
- Mode III is a shear-mode crack (tearing), where the crack surfaces move relative to one another and parallel to the leading edge of the crack. This sort of crack also cannot propagate in its own plane.

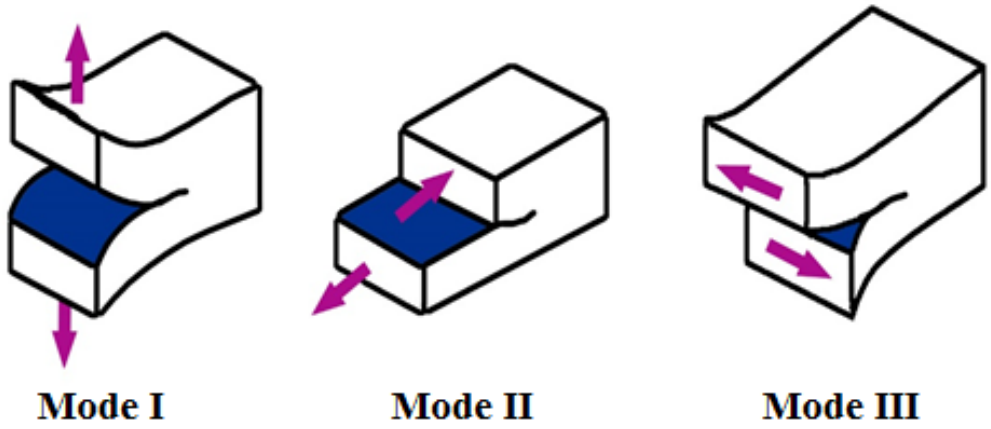

Figure 2.1.1. Three basic fracture modes of loading, their geometry and surface displacement.

Hydraulic fracturing experiments are used to study fracture initiation pressure and propagation orientation, and for determining in-situ principal stresses (Backers 2005). The breakdown pressure is calculated using Griffith's criterion, which assumes fracture is initiated when maximum tangential stress on the borehole wall reaches apparent tensile strength (Griffith 1921). According to Griffith, there is a large discrepancy between theoretical strength and experimental fracture strength of a brittle material. This discrepancy is due to the inherent defects in brittle materials, such as pre-existing micro-cracks. Under triaxial compression, local tensile fracture is initiated near the tips of the microcracks (Griffith 1921). The Griffith's criterion predicts macroscopic failure based on micromechanics description and is quantified by:

$$\sigma_t = \sqrt{\frac{2E\gamma}{\pi a_0}} \tag{2.1.1}$$

where σ_t is the tensile stress necessary to cause crack growth, E is Young's modulus, γ is fracture surface energy, and a_0 is the half-length of the initial crack.

2.2 Fracture Toughness and Its Controlling Factors

Stress Intensity Factor (SIF) is a critical parameter in fracture mechanics to predict the stress intensity near the tip of a crack that relates to remote load, crack size, and structural geometry (Backers 2005). After reaching its critical value, which is defined as fracture toughness, rock will be fractured. As a result, fracture toughness represents the ability of rock to resist fracture propagation from preexisting cracks (Zhang 2002; Backers 2005; Wang et al. 2007). It has been proven that the higher the fracture toughness, the higher the breakdown pressure. For Mode-I fracture, crack initiation occurs once *SIF* reaches fracture toughness (Backers 2005).

Fracture toughness can be measured via various methods, such as: Chevron Notched Short Rod (CNSR) Method, Chevron Notched Semicircular Bend (CNSCB) Method, Chevron Notched Brazilian Disk (CNBD) Method, etc. Generally speaking, fracture toughness measurement of rock is more difficult and complex than other rock mechanical properties testings. To reduce the turnaround time and expense, many studies have been conducted to derive some empirical relationship between fracture toughness and some physical-mechanical properties of rock, such as Young's modulus, Poisson's ratio, hardness, grain size, tensile strength, uniaxial compressive strength, and velocity of primary acoustic wave (Brown and Reddish 1997; Al-Shayea et al. 2000; Zhang 2002, Backers 2005; Nasseri and Mohanty 2008). However, due to the limited resources of fracture toughness measurements reported in the literature, multi-verifications are indeed necessary. A problem that exists here is that many parameters mentioned above (i.e., Young's modulus, Poisson's ratio, tensile strength, etc.) are anisotropic in both vertical and horizontal directions. As a result, fracture toughness is

also anisotropic. Moreover, the size and orientation of microstructural features also greatly affect the anisotropy effect of rock fracture toughness (Nasseri et al. 2005). Since natural fractures are very common and also complex in unconventional shale reservoirs, the degree of fabric anisotropy is even locally different at small scales. Fracture toughness anisotropy as a result is an important concept in hydraulic fracturing. Unfortunately, knowledge about the effect of fracture toughness anisotropy on hydraulic fracturing is still very limited in the literature.

2.3 Tensile Strength and Its Controlling Factors

The studies on shale tensile strength and its controlling factors are limited in the literature. This section gives a critical review of tensile strength anisotropy observed in the Woodford shale in a study by Sierra (2011) and which factors show a positive potential in controlling tensile strength. The emphasis here was also to find key parameters that might potentially affect tensile strength of shale. The effects of several factors, including bedding orientation, TOC, clay content, non-clay minerals content, porosity, etc., on shale tensile strength are reanalyzed and show some potential for future analyses.

In the study by Sierra et al. (2010), preserved Woodford shale samples at different depths were obtained from a shallow research well in Oklahoma and prepared for the Brazilian Tensile tests and the Chevron Notched Semicircular Bend (CNSCB) tests, both under tensile regime. For each selected depth, a sample was loaded parallel to the bedding plane ($\theta_b = 90^o$) while the other sample was loaded perpendicular to the bedding plane ($\theta_b = 0^o$) (Figure 2.3.1).

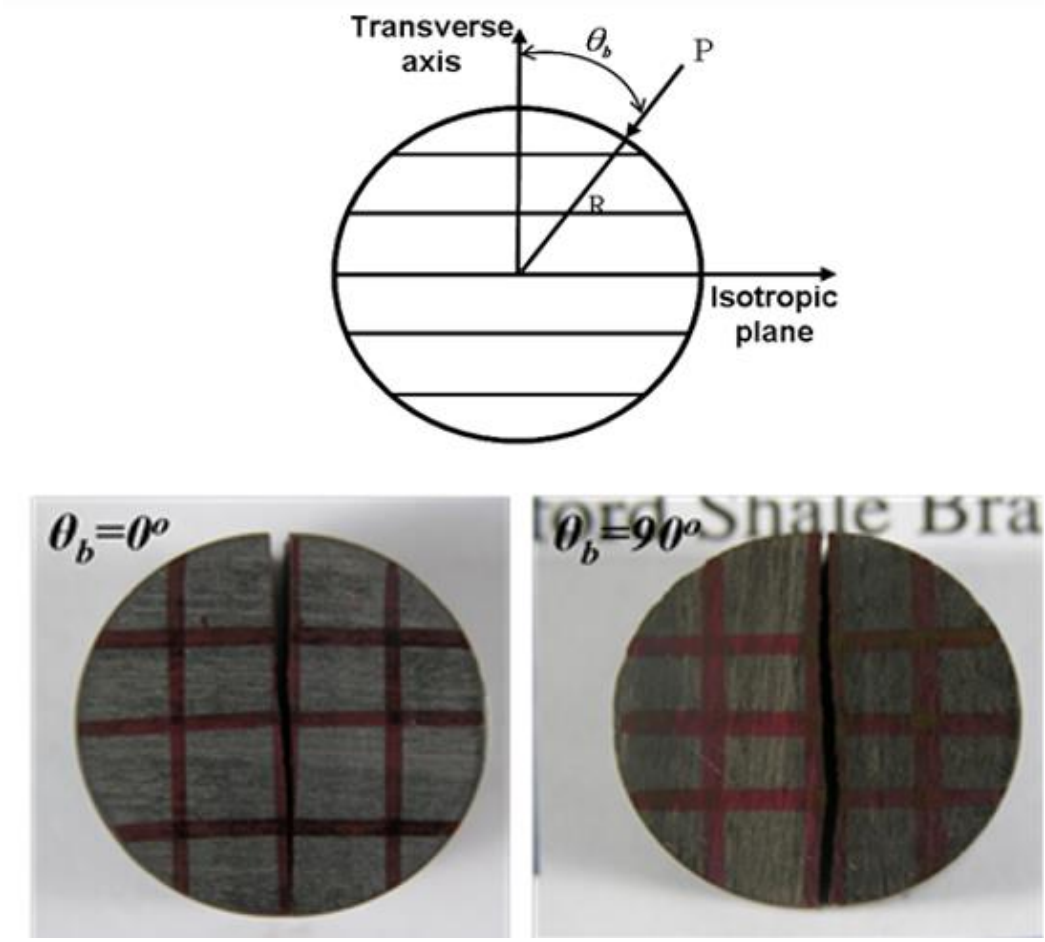

Figure 2.3.1. Tested Woodford shale samples in the study by Sierra (2011). For each selected depth, a sample was loaded parallel to the bedding plane (θ_b = 90º) while the other sample was loaded perpendicular to the bedding plane (θ_b = 0º).

The Brazilian test results (Table 2.3.1) show a clear anisotropic nature of Woodford Shale tensile strength, as can be seen in Figure 2.3.2. Tensile strengths of samples loaded parallel to the bedding plane (θ_b = 90º) are approximately half of those of samples loaded perpendicular to the bedding plane (θ_b = 0º).

Table 2.3.1. Brazilian tensile strength of Woodford shale at selected depths (Sierra et al 2010).

Depth (m)	Load Direction (rel. to bedding)	Max. Load (N)	Tensile Strength (MPa)

33.81	⊥	3747	12.8
	//	2351	6.2
36.85	⊥	3556	12.7
	//	1989	7.4
41.36	⊥	3347	11.4
	//	1956	5.0
44.28	⊥	3140	11.2
	//	1920	5.1
50.59	⊥	3276	11.7
	//	1609	4.4

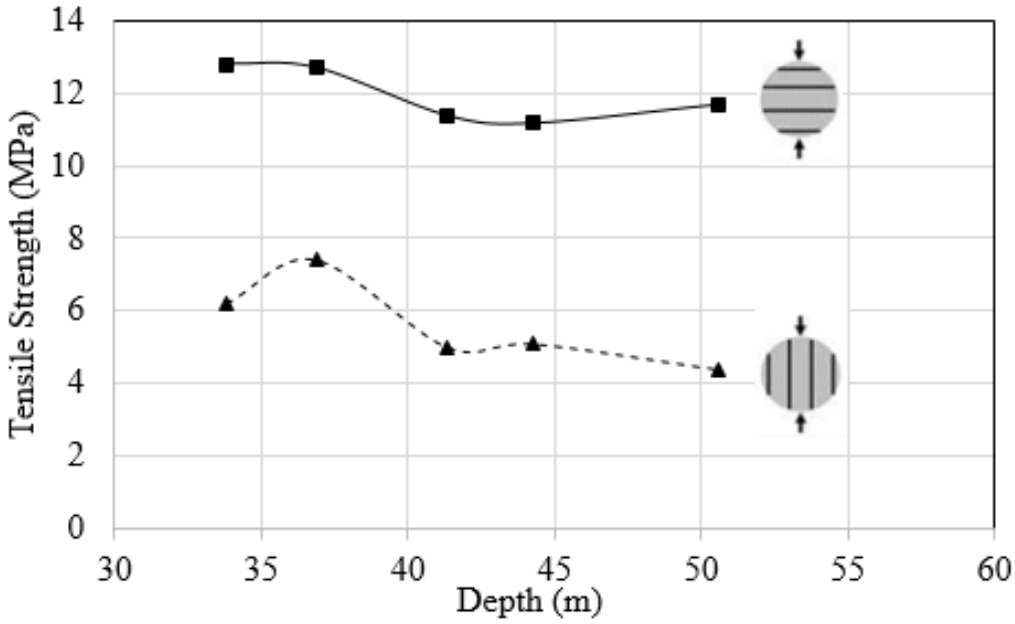

Figure 2.3.2. Brazilian tensile strength of Woodford samples with loading directions normal and parallel to bedding planes (data was taken from Sierra et al. 2010).

Sierra (2011) suggests that rock fabric (laminations and horizontally-oriented clay micro-fabric) rather than shale mineralogy has a direct influence on rock strength. Following a widely used correlation in the industry, the vertical unconfined compressive strength (UCS) is extrapolated to relate to the *vertical* tensile strength (loaded parallel to the bedding planes, $T_{//}$) by a factor of 0.1 (Sierra 2011). For the

lateral tensile strength (loaded perpendicular to the bedding planes, T_p), some empirical relations were made in terms of the upscaled dynamic Young's modulus, E_1 and E_3. Figure 2.3.3 presents the results of these correlations (Sierra 2011).

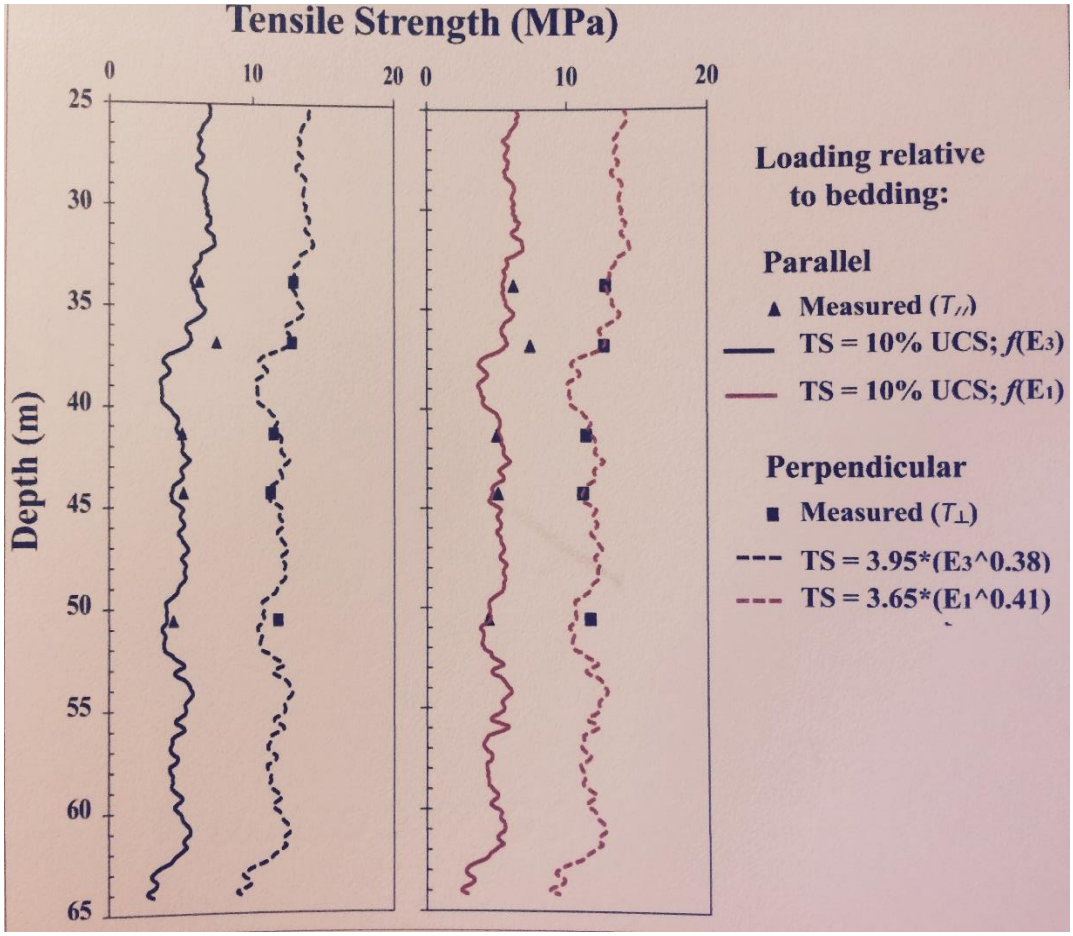

Figure 2.3.3. Tensile strength estimation from UCS and upscaled E_1 and E_3 of Woodford shale (Sierra 2011). The vertical unconfined compressive strength (UCS) is used to estimate the vertical tensile strength (loaded parallel to the bedding planes, $T_{//}$) by a factor of 0.1. For the lateral tensile strength (loaded perpendicular to the bedding planes, T_p), empirical relations were made in terms of the upscaled dynamic Young's modulus, E_1 and E_3.

As can be seen in Figure 2.3.3, correlation of the vertical and lateral tensile strengths, respectively, show a promising result in which the measured values for tensile

strength and their predicted values do not differ significantly. However, some limitations still exist in these correlations, including:

- The input of vertical UCS requires laboratory measurements; thus, not only the Brazilian tensile strength test but the uniaxial compressive strength test also require available samples to do lab experiments. As a result, UCS input for the correlation with $T_{//}$ is more likely depth selected and would not be available for all well sections.
- The estimation of lateral tensile strength (T_p) is mainly dependent on an empirical relation with upscaled dynamic Young's modulus E_1 and E_3. However, these correlations might be locally applicable for Woodford shale only. Thus, in order to get a more common and general correlation that will work for many major organic-rich shales, refinements are indeed necessary.

Based on the limitations mentioned above, I decided to change the direction of data analysis. Instead of modifying and coming up with a better(?) correlation with either vertical/lateral UCS or upscaled dynamic Young's modulus as presented in the study by Sierra (2011), I reviewed some of the physical and mineralogical parameters reported in this study and observed the behavior of these parameters with lateral/vertical tensile strengths. Meaning that I plotted the calculated vertical and lateral Woodford shale tensile strengths versus non-clay mineral content, clay content, TOC, and porosity, respectively, and show the results in Figure 2.3.4. Some major observations include:

- ✓ Lateral tensile strengths (T_p) of samples loaded perpendicular to the bedding planes are higher than those of samples loaded parallel to the beddings ($T_{//}$).

- ✓ For the group of samples loaded parallel to the bedding plane: relationships between $T_{//}$ and non-clay content, porosity, and especially clay content are significantly pronounced. The fact that the correlation of $T_{//}$ with clay content shows a significantly high value of R^2 (~0.92) supports the simple idea that the granular nature of shale is a result of the depositional structure of clay particles, ranging from highly ordered sheet packages to wavy flake structures (Abousleiman et al. 2016). As a result, tensile strength of this group probably is more likely controlled by clay content and/or non-clay mineral content.
- ✓ For the group of samples loaded perpendicular to the bedding plane: correlations between T_p and four parameters mentioned above are highly questionable due to the low values of R^2. In fact, none of these correlations have the value of R^2 exceeding 0.6. It is also doubtful that either shale composition or porosity solely controls lateral tensile strength. As a result, prediction of T_p might require rather a single yet more representative parameter than those parameters acting individually like non-clay mineral content, clay content, TOC, and/or porosity.

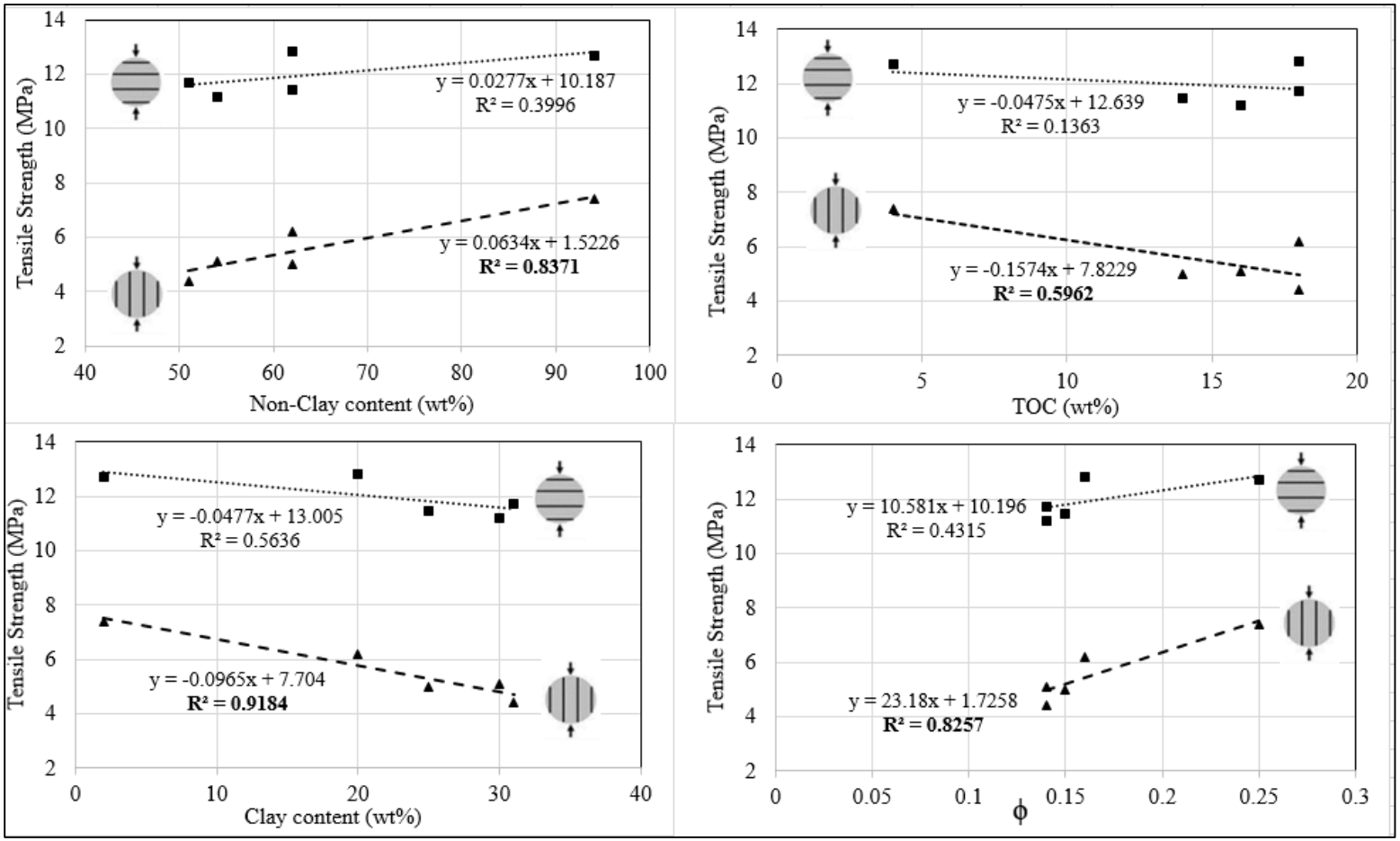

Figure 2.3.4. Tensile strength of tested Woodford samples versus non-clay content, clay content, TOC, and porosity (data was taken from Sierra et al. 2010).

By incorporating all of these factors (clay content, non-clay content, TOC, and porosity) into a single property defined as clay packing density, the main constituents of shale and its morphology, which is quantified by porosity, are condensed and representative of the nano-granular signature of shale (Ortega et al. 2007). The total porosity, ϕ, was translated into the clay packing density by

$$\eta = 1 - \frac{\emptyset}{1 - f_{inc}} \tag{2.3.1}$$

where f_{inc} is the non-clay inclusion fraction known from mineralogy, η is the clay packing density, m is mass percentage, and ρ is density.

$$f_{inc} = (1 - \emptyset)\frac{\sum_{k=1}^{total\ non-clay} \frac{m_k}{\rho_k}}{\sum_{k=1}^{total\ non-clay} \frac{m_k}{\rho_k} + \sum_{l=1}^{total\ clay} \frac{m_k}{\rho_k}} \tag{2.3.2}$$

This clay packing density expression describes how tightly clay poly-crystals are packed together in the granular matrix of shale minerals. Prior investigations show a correlation between the degrees of anisotropy with clay packing density; i.e., the higher the clay packing density, the more pronounced the anisotropy (Ulm and Abousleiman 2006). The Woodford shale data set, again, confirms that tensile strength anisotropy ratio ($T_p/T_{//}$) of Woodford shale possesses an increasing trend with increase in clay packing density, as shown in Figure 2.3.5 (Sierra et al. 2010). Despite the limited number of tests available in this study, results show that the anisotropic nature observed in tensile strength is dependent on clay packing density.

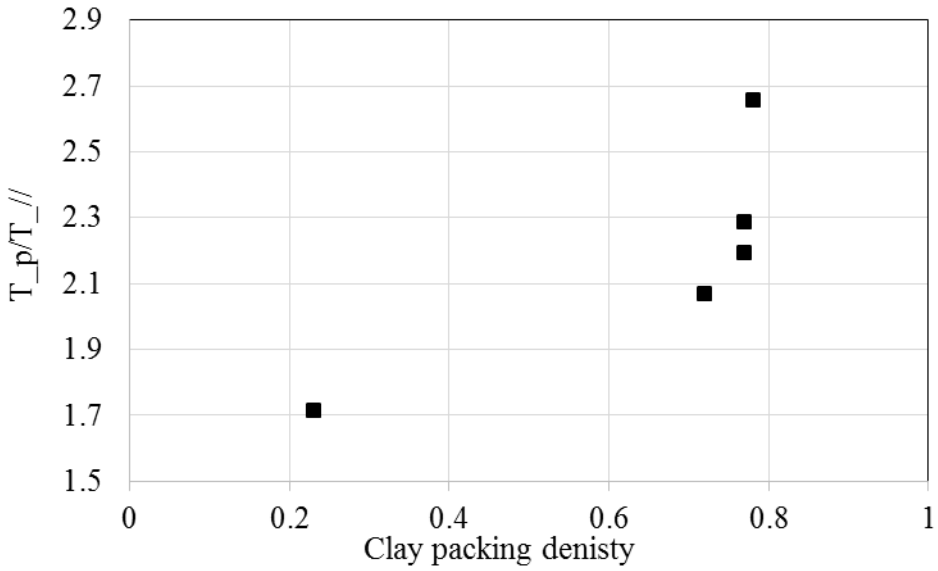

Figure 2.3.5. Tensile strength anisotropy ratio ($T_p/T_{//}$) versus clay packing density (data was taken from Sierra et al. 2010).

2.4 The Granular and Polymer Nature of Shale

Recalling from Figure 2.3.3, correlations between lateral tensile strength (of Woodford samples loaded perpendicular to bedding planes) with clay content, non-clay minerals content, TOC, and porosity are not significantly pronounced. Considering that Woodford shale is known for its anisotropy as an organic-rich shale, the granular and polymer nature of shale might be worth revisiting. Organic-rich shale anisotropy not only results from mode of deposition, bedding planes, micro-fractures and/or nanoclay grain shape and clay packing density (Abousleiman et al. 2016), but also from the presence of kerogen interlayered with clay minerals, as can be seen in Figure 2.4.1. While it is common to have kerogen dispersed in the shale structure, the Woodford shale shows pronounced interlayered kerogen strings occurring in the granular mineral matrix.

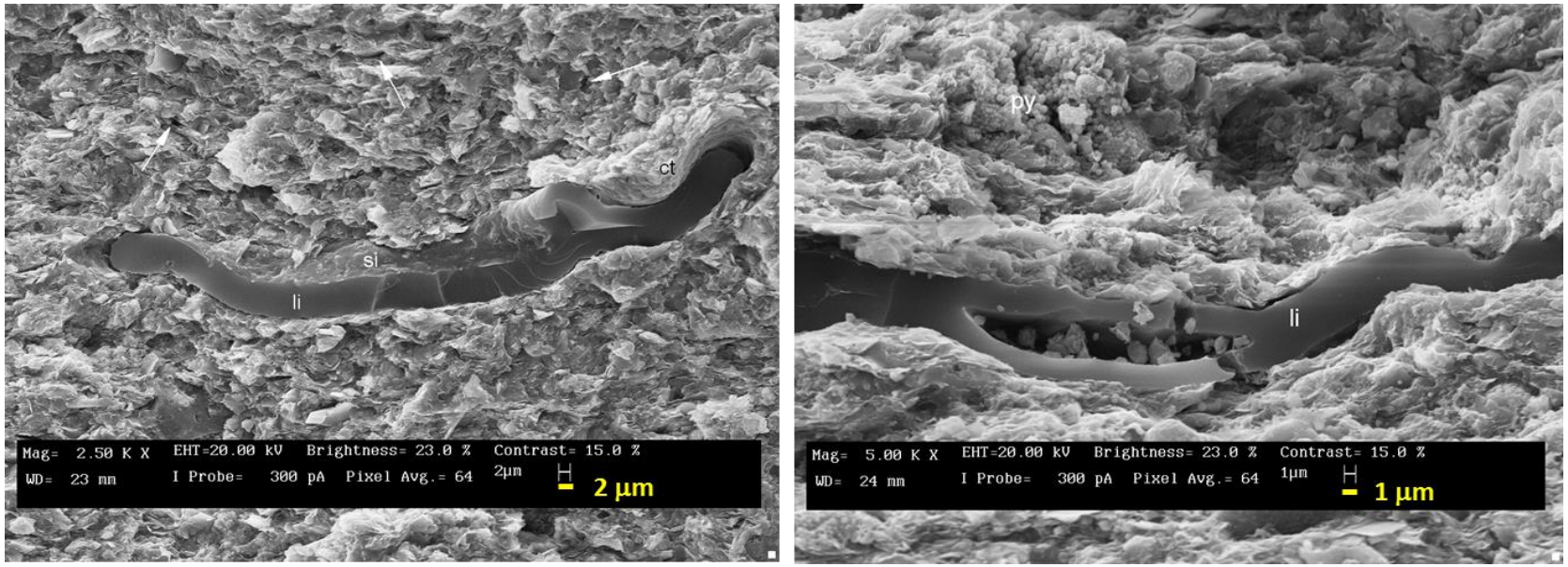

Figure 2.4.1. SEM images of Woodford shale highlighting the intertwined nature of minerals and kerogen (black polymer looks like ribbons) (Abousleiman et al. 2016).

Prior to kerogen receiving as much attention as it has recently, Ortega et al. (2007), using nano-indentation technique, attempted to measure shale mechanics at the smallest possible "porous unit" of a mudstone, i.e., attempting to identify the scale of the Representative Elementary Volume (REV) of fluid-filled shale composites. The study can be summarized in a way that the 'heterogeneous' mechanical behavior of shale composites can be estimated from the 'homogenized' mechanical characteristics of homogeneous phases within this REV. The heterogeneity of shale is due to local non-clay minerals such as quartz, calcite, and pyrite, and clay minerals intertwined with string-shaped polymer kerogen at nano-, micro-, and macro-levels (Abousleiman et al. 2016).

Similar to the multiscale structure of kerogen-free shale, a kerogen-rich shale multiscale mechanical structure is summarized in Figure 2.4.2 (Abousleiman et al. 2016). This model translates the heterogeneous nature of shale into different levels of predictive, homogeneous shale 'poly-crystals.' First, Level 0, the scale of elementary clay-silt particles with or without organic molecules, has been classified as the fundamental scale of clay mineralogy. Due to the small nature of clay particles as well as the organic molecules in pure solid crystals, direct measurements of mechanical properties and strength are still very limited and possess many difficulties. Level I is the scale of porous clay composite that may interweave with nano-porous organic matters. This level can manifest the varying configurations of porous clay composite and organic matter at the sub-micrometer scale, which is also the scale of advanced observational methods like SEM. Using mercury injection porosimetry method, most of the measured total effective porosity in shale comes from pores between clay sheets with pore access

radii of nanometers scale. From level II up to level III, porous clay fabric is intertwined with kerogen in the micrometer to millimeter range. At this scale, micro-pores, if present, are distributed throughout an abundant matrix of non-clay inclusions and porous clay. As a result, the future model predicting tensile strength of shale needs to link those different scales together so that the heterogeneity can be minimized at most. The bridge here is clay packing density, which has already been mentioned in Section 2.3. Alternatively, a parameter called clay phase porosity ($\phi_{clay} = 1 - \eta$) will be applied in future analysis; more details are available in Section 3.3.

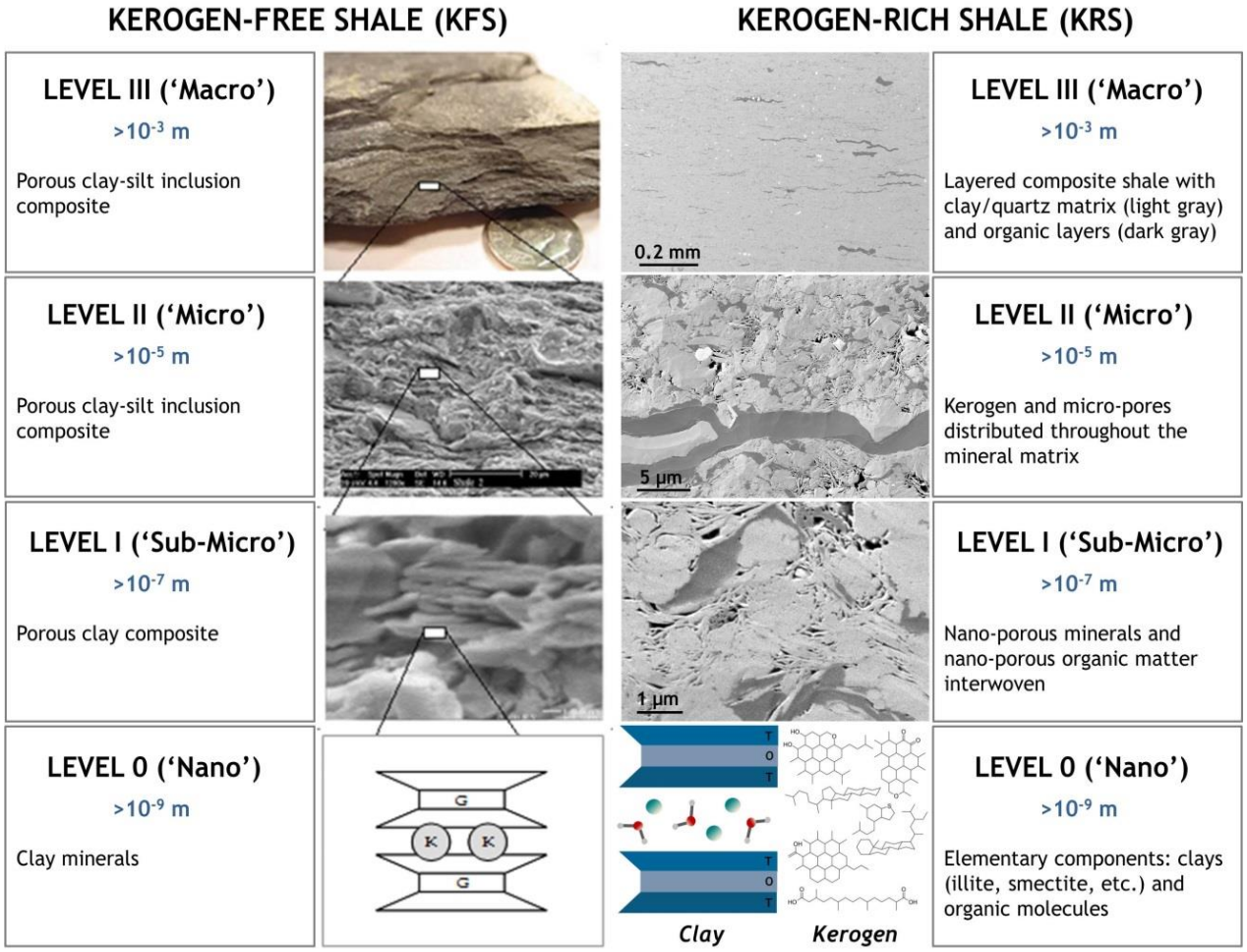

Figure 2.4.2. Multi-scale structure model of shale (Abousleiman et al. 2016).

2.5 The Nature of Pores – Tensile Failure Patterns in Organic-rich Shale: Simple or Complex?

Most major unconventional shale reservoirs share common mineral composition such as non-clay components like quartz, feldspar, pyrites (QFP), and clay minerals like kaolinite, illite, smectite, etc. and particularly for organic-rich shale, organic matter such as kerogen (~5-6 wt%, or ~10-12 vol%) and bitumen (Slatt and O'Brien 2011; Abousleiman et al. 2016). The pore structure of shales also affects geomechanical properties (Slatt and Abousleiman 2011). In kerogen-free shale, through the mercury intrusion porosimetry (MIP) technique, it has been determined that most porosity in shale is attributed to the spaces between clay sheets, with characteristic pore access radii of some nanometers to micrometers (Ortega et al. 2007). Although these matrix-based pores are indeed best viewed with high-resolution imaging techniques, they are not the only type of pores found in shale. In kerogen-rich shale, besides the regular pores residing in the granular matrix, organic matter contains pores as well. Field emission scanning electron microscopy (FESEM) along with incremental, argon ion-milled surfaces has allowed the observation of significant "organo-porosity" within kerogen, which is generated during burial maturation (Slatt and Abousleiman 2011). Organoporosity is reported in some highly mature gas shale; for example, the Barnett shale, as it displays abundant organic matter-hosted pores with less matrix-based porosity (Slatt and O'Brien 2011). Those organopores are at nanometer scale and are generally isolated. In fact, the degree of connectivity of these pores within the polymer kerogen body and the granular matrix of shale at micrometer scale is still questionable to the contribution of these pores to permeability (Slatt and O'Brien 2011) and if not

tensile fracture development in shale. It is, therefore, not so surprising if the regular matrix-based pores may have more controls on tensile fracture development for oil and wet gas production from relatively low-maturity shale plays, such as the Woodford shale.

Using standard SEM techniques, Slatt and O'Brien (2011) revealed the following matrix based pore types in many shales:

- porous floccules: typical flocculated clay microfabric are common in Woodford shale and Barnett shale;
- porous fecal pellets;
- fossil fragments such as sponge spicules, radiolarian, and *Tasmanites*;
- porous mineral grains such as pyrite framboids;
- microchannels within shale matrix;
- fractures at micron and larger scales that often crosscut shale bedding planes.

Among these pore types in organic-rich shale, microchannels and microfractures in shale matrix are considered to be a significant contributor for matrix-based porosity. Microchannels commonly are sinuous, discontinuous, and are generally less than 0.5 cm (<0.2 in.) in length (Slatt and O'Brien 2011). In addition, microfractures in some of the organic-rich shale such as Woodford shale, Eagle Ford shale, and Barnett shale are abundant; in fact, fractures in these kinds of shale occur at a variety of scales (Slatt et al. 2012; Gale et al. 2007).

To understand the tensile failure pattern in organic-rich shale, a question that needs to be addressed is "Where do tensile fractures and failures occur in the granular nature of shale and its intertwined polymer kerogen?"

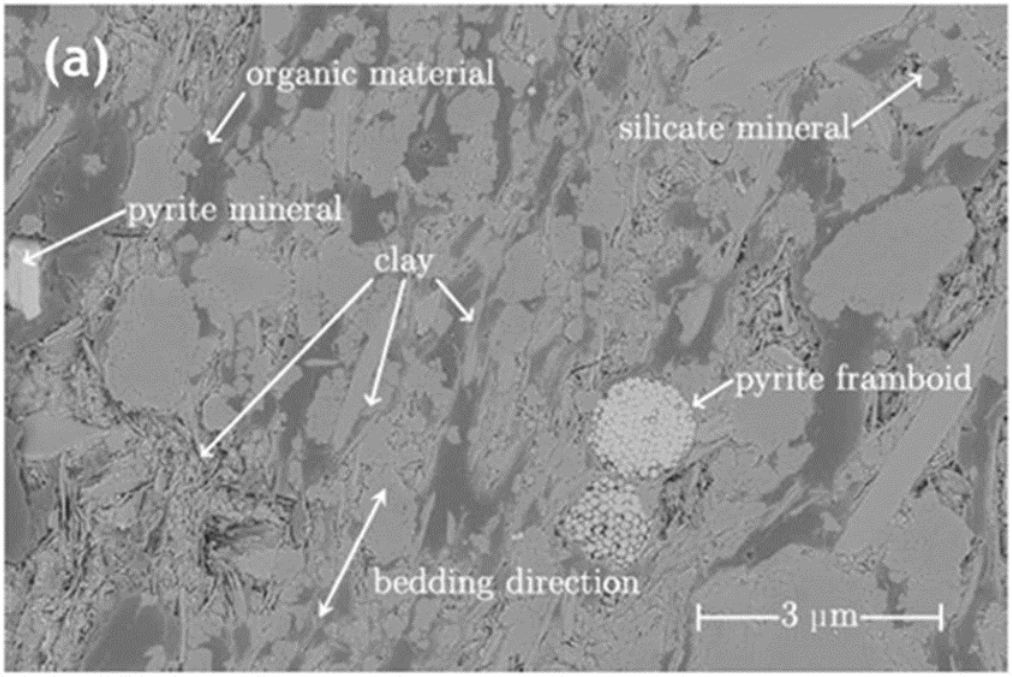

Figure 2.5.1. Woodford shale SEM image shows a polished surface with organic material which includes 1 µm size diameter pyrite framboids, silicate, clays, etc. (Abousleiman et al. 2016)

Figure 2.5.1 presents a SEM image of a Woodford shale sample showing various mineral and non-mineral phases. The organic matter possesses globular structure or string-like structure and is interwoven with clay and non-clay minerals. In a recent study by Abousleiman et al. (2016), it was confirmed that this organic matter has polymer-like qualities such as high tensile strength and even far exceeds the tensile strength of the rock matrix. In this study, loading and failure process of a micro-sized beam of Woodford shale in tensile loading mode was observed inside the SEM with a small-scale nano-indenter. The micro-sized beam in Figure 2.5.2 shows a polymer-based rod-like object stretching and yet still holding the failed-microbeam to the severed support. This polymer-based rod-like object is a lenticular organic matter that is woven within the shale mineral matrix. The size of these kerogen strings can be more

than 100 μm in length and 5-10 μm in thickness. They can be embedded inside the micro-sized beam or can even reach out to the micro-cantilever beam fixed support. Thus, even though the granular shale matrix is broken, the micro-beam still hangs on to the support. In other words, the polymer-like kerogen string keeps the beam attached to the support after a total tensile failure of the micro-beam (Abousleiman et al. 2016)

Moreover, I also observed the tensile failure patterns of an Inclined Direct Shear Testing Device (IDSTD) tested Woodford shale sample from a study by Tran (2009). This SEM image was taken on the failure surface of an IDSTD tested sample to confirm the hypothesis about micro fractures forming parallel to sample axis of symmetry. Figure 2.5.3 is a SEM image showing the existence of vertical micro- and nano-fractures on some particles. The fractures result from tensile stress forming along the cleavage plane of the particle (mineral) due to application of axial loading, which is similar to the Brazilian test (Tran 2009).

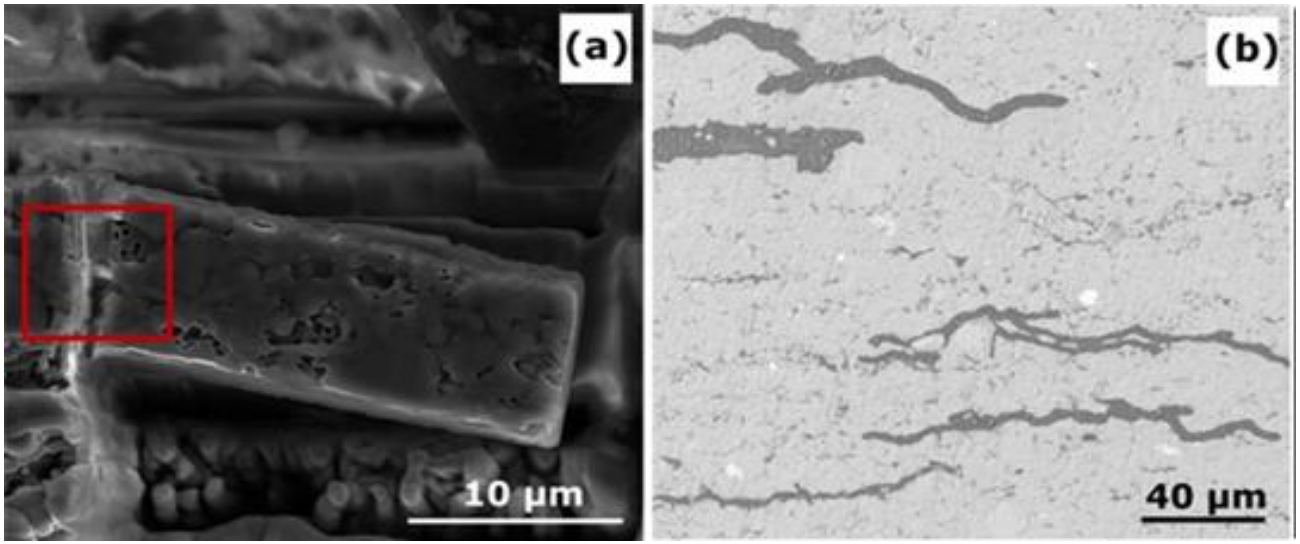

Figure 2.5.2. (a) SEM image of the micro-beam T1 at failure with a red square highlighting the string organic matter embedded into the micro-beam support; (b) SEM image of Woodford shale from the same horizon with the interlaced lenticular kerogen in dark colors, (c) the full loading-displacement curve of the micro-beam T1(Abousleiman et al. 2016).

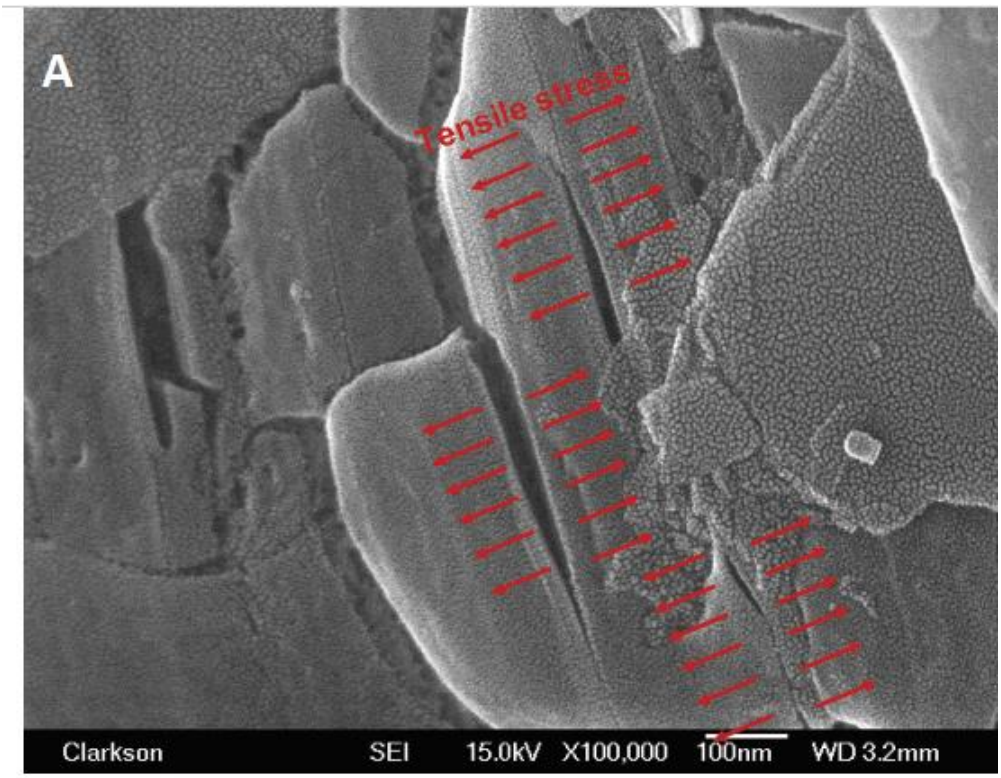

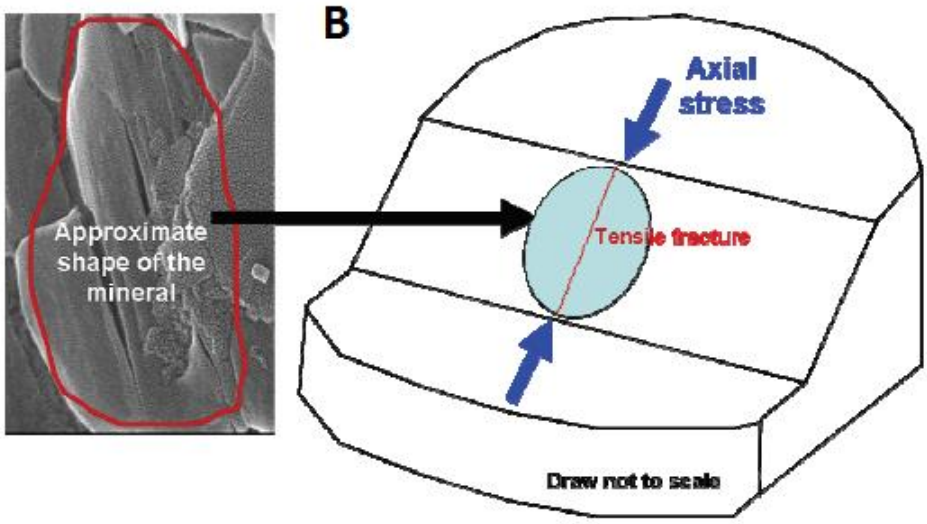

Figure 2.5.3. SEM images showing (A) tensile fractures on a mineral on the failure plane of an IDSTD tested Woodford shale and (B) illustration of how tensile

fractures are formed on particle under axial loading (Tran 2009, Slatt Abousleiman 2011).

2.6 Micromechanics-Derived Scaling Relations for Uniaxial Tensile Strength of Brittle Porous Polycrystals

As mentioned in Section 2.5, the regular matrix-based pores may have more controls on tensile fractures initiation and development on shale. Fritsch et al. (2013) used a so-called homogenization method to upscale poroelasticity and strength of brittle porous polycrystals. Even though the scope of this study applies to ceramic geological and biological materials, it might resemble the upscaling exercises that many petroleum scientists and researchers have been studying and applying to identify shale mechanical properties. In short, the homogenization method is built upon an infinite amount of nonspherical (needle or disk-shaped) solid crystal phases and a spherical pore phase (Fritsch et al. 2013). To some extent, this might be considered an ideal structure of shale in which the clay and non-clay minerals are solid 'shale crystals' and pores in shale are spherical. Nonetheless, it might give some insight into the study of tensile strength and its controlling factor, as presented in the following sections.

A poromicromechanical analysis by Fritsch et al. (2013) of brittle porous polycrystals with either *needle*- or *disk*-shaped solid crystals concludes that the uniaxial tensile strength, $\sum^{ult,t}$, of a nonpressurerized porous polycrystals is a function of the form:

$$\sum^{ult,t} = \mathcal{F}_{\sum^{ult,t}}\left(E_s, \nu_s, \sigma_s^{ult,t}, \sigma_s^{ult,s}, \phi\right). \tag{2.6.1}$$

The study shows that the normalized tensile strength of needle- or disk-shaped porous polycrystals, $\frac{\sum^{ult,t}}{\sigma^{ult,t}}$, decreases over-linearly with porosity. These approximations can be estimated by either power law functions,

$$\frac{\sum^{ult,t}}{\sigma^{ult,t}} \approx \alpha(1-\phi)^{\beta} = \frac{\sum^{ult,t}}{\sigma^{ult,t}} \tag{2.6.2}$$

or alternatively, by polynomial functions,

$$\frac{\sum^{ult,t}}{\sigma^{ult,t}} \approx A(1-\phi)^4 + D(1-\phi)^3 + C(1-\phi)^2 + D(1-\phi) + E = \frac{\sum^{ult,t,app}}{\sigma^{ult,t}} \tag{2.6.3}$$

where $\Sigma^{ult,t}$ is tensile strength of porous polycrystals and $\sigma^{ult,t}$ is tensile strength of crystal in solid phase.

To be clear, Figure 2.6.1 and Figure 2.6.2 show normalized tensile strength of *needle*-based and disk-based porous polycrystals, respectively, as a function of porosity. Experimental data of hydroxyapatite and gypsum are also included to verify the reliability of the disk-based model, as well. The fact that the normalized tensile strength of porous polycrystals decreases as a function of porosity means the uniaxial tensile strength of porous polycrystals acts linearly with the tensile strength of the solid crystals (Fritsch et al. 2013). The result is promising, such that porosity might be a significant parameter that controls tensile strength of many types of shale.

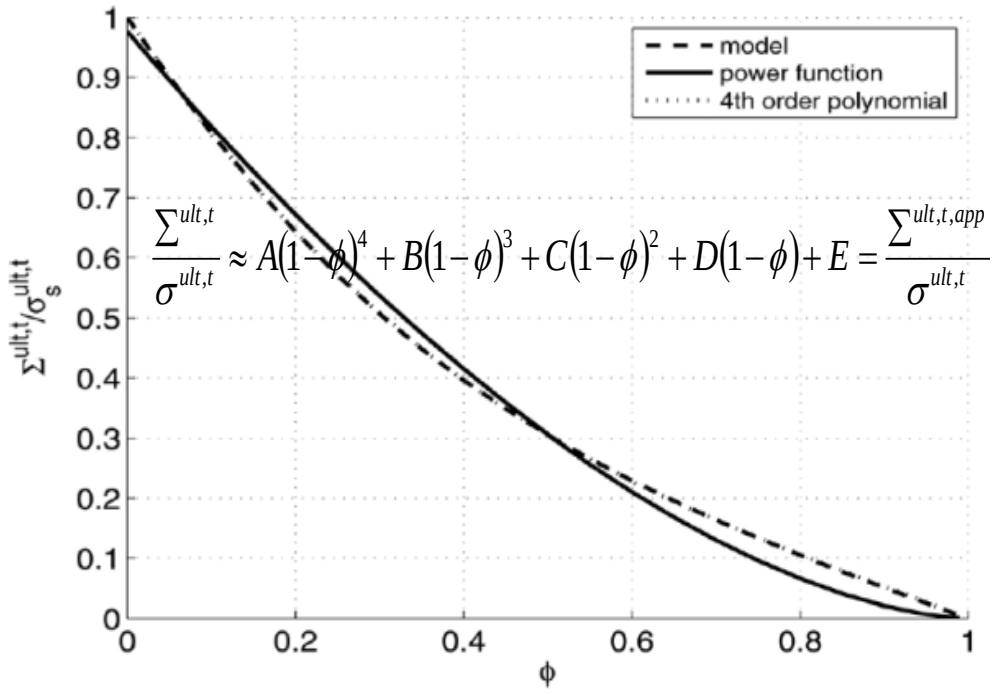

Figure 2.6.1. Normalized tensile strength of *needle*-shaped polycrystals (modified from Fritsch et al. 2013).

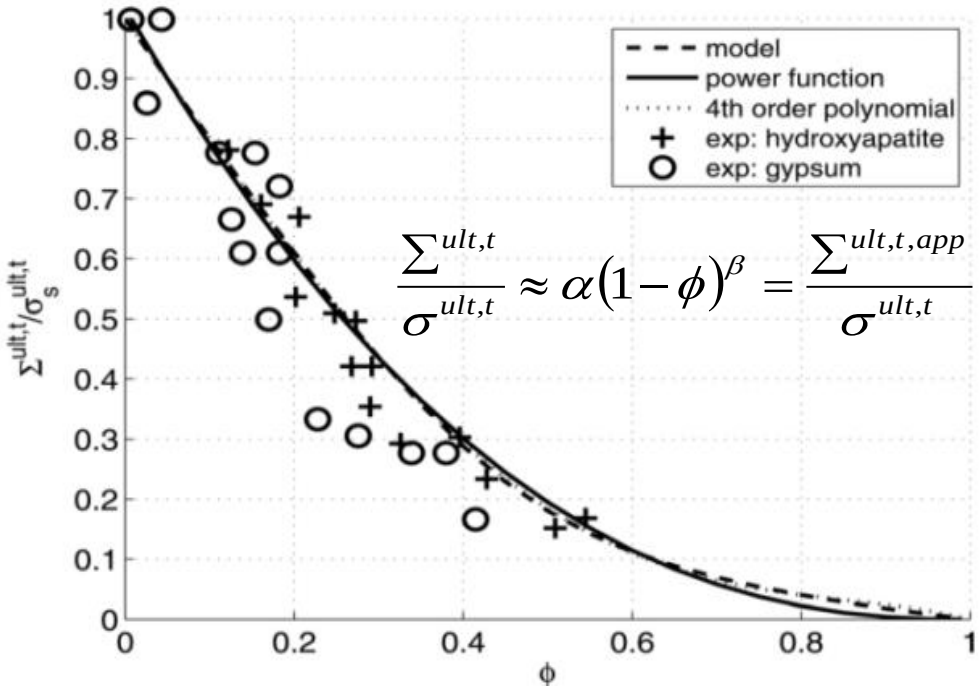

Figure 2.6.2. Normalized tensile strength of *disk*-shaped polycrystals (modified from Fritsch et al. 2013).

As mentioned at the beginning of this section, an ideal structure of shale in which the clay and non-clay minerals are solid 'shale crystals' and pores in shale are spherical might act as a simple analog of kerogen-free shale (KFS). Regardless of the shape of the solid crystals, both Figures 2.6.1 and 2.6.2 clearly show a decreasing trend of the normalized tensile strength, $\frac{\sum^{ult,t}}{\sigma^{ult,t}}$, as a function of porosity. Therefore, it would be interesting to see if the uniaxial tensile strength, $\sum^{ult,t}$, of kerogen-free shale can be written in a function of the form

$$\Sigma_{KFS}^{ult,t} = \mathcal{F}_{\sum^{ult,t}}\left(E_s, \nu_s, \sigma_s^{ult,t}, \sigma_s^{ult,s}, \phi\right). \tag{2.6.4}$$

For kerogen-rich shale, how is the effect of kerogen incorporated into the above expression? In order to do that, the bridge that connects all of the main constituents and

porosity in shale defined as clay packing density (or clay phase porosity) should be revisited.

CHAPTER 3: TENSILE STRENGTH MODELING

3.1 Experimental Description

As discussed in Chapter 2, effect of bedding plane or lamination plays a significant role in controlling vertical tensile strength of shale ($T_{//}$). Moreover, Brazilian tensile strength tests are conducted on cores retrieved from deep rock formations; that means the tests usually are not conducted at in-situ conditions. For cores retrieved from the subsurface, most damage comes from fractures and microcracks developed along the shale bedding planes. As a result, due to the limitations in the core retrieving process, the apparent tensile strengths of samples loaded parallel to the beddings ($T_{//}$) certainly are affected by human factors rather than other intrinsic minerals' properties. In other words, test results sometimes are underestimated in laboratory measurements; thus, vertical tensile strengths of samples loaded parallel to the beddings ($T_{//}$) are generally lower than those of samples loaded perpendicular to the bedding planes (T_p).

To some extent, lateral tensile strengths (T_p) might be a better choice of data collection for the scope of this study, based on the interactions and spatial distribution of non-clay minerals, clay minerals, kerogen, and pores in shale to predict its tensile strength. As I observed the correlations between lateral tensile strength, T_p, with non-clay minerals content, clay content, TOC, and porosity, respectively, in section 2.3, it was suggested that all of these individual components might add up to a single yet more representative parameter called clay packing density. This property describes how tightly the clay particles are packed together in shale minerals matrix.

To prepare a data set including both kerogen-free shale and kerogen-rich shale for this model, most of the data here (except for the Pierre shale and Hydro shale) were

collected from the literature: Lin (1983), Sierra et al. (2010), Lai et al. (2015), and Rybacki et al. (2015). Kerogen-free shale include Mesaverde shale and Pierre shale. The group of kerogen rich-shale consists of Woodford shale, Eagle Ford shale, Hydro shale, Mancos shale, Barnett shale, Dotternhausen (Posidonia) shale, and Wickensen (Posidonia) shale. Ultimate tensile strength was measured by conducting Brazilian indirect tensile strength tests. The setup, sample preparations, and calculation of tensile strength follows instructions according to American Society for Testing and Materials (ASTM) D3967-08 standard.

In addition to the Brazilian indirect tensile strength tests, mineralogy information of each sample was determined by X-ray diffraction (XRD) mineralogy analysis. Porosity was measured using mercury injection porosimetry. This method estimates a majority of macropores (>50 nm), which is a common pore size in the shale minerals matrix. As stated in Section 2.5, because the regular matrix-based pores (excluding the disconnected organoporosity in kerogen body) may have more controls on tensile fractures development in organic-rich shale, mercury injection porosimetry is considered to be an appropriate method to measure porosity for the scope of this study.

3.2 Clay Geometry: *Needle*- or *Disk*-Shaped? Does It Matter?

Shale is composed of both matrix and inclusions; these inclusions can be either solid granular materials (quartz, pyrite, feldspar, etc.) or pores and fractures filled by gas, oil or water, or a combination of both. The matrix contains clay minerals, such as illite, chlorite, smectite, kaolinite, etc. In particular, an important observation of clay minerals shows that they might be either needle-based or disk-based poly-crystals. Figure 3.2.1 shows four SEM images of common clay minerals found in shale such as

kaolinite, illite, chlorite, and smectite. While kaolinite crystals exhibit a uniform hexagonal shape and illite appears to look fibrous, smectite particles have a peculiar shape and appear in a network, which makes it difficult to define a unique shape for them. As a result, even though the shape of clay minerals does not perfectly resemble a needle or disk, we might consider that shale contains a clay mixture of either type or both types of these polycrystals.

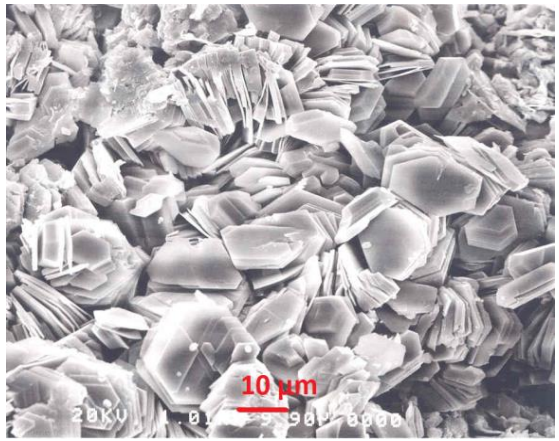

Kaolinite

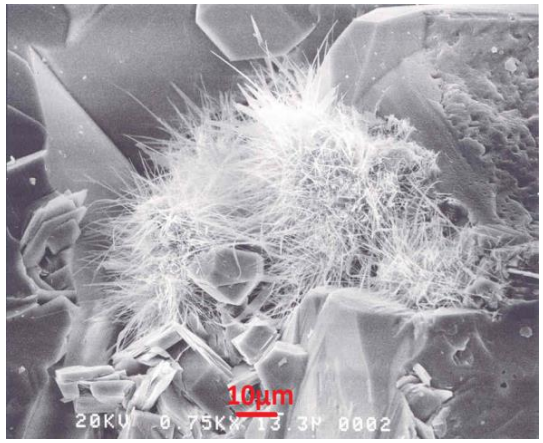

Illite

Chlorite

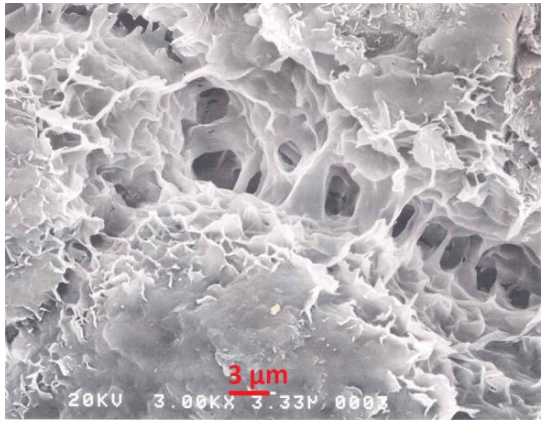

Smectite

Figure 3.2.1. SEM images of common clay minerals in shale (PetroTech Asscociates 2016). http://www.petrotech-assoc.com/prod01.htm.

3.3 Clay Phase Porosity

Recalling from Section 2.6, Fritsch et al. (2013) applied total porosity as the input for the numerical model predicting tensile strength of brittle porous polycrystals. However, as the clay minerals phase was hypothesized to play a dominant role in controlling tensile failure in shale, instead of using total porosity as input, I used porosity of clay phase (i.e., clay phase porosity). This clay phase porosity parameter was mentioned in the study by Sierra et al. (2010): in kerogen-free shale, clay phase porosity was computed by converting total effective porosity through the volume fraction of non-clay mineral phases (quartz, feldspar, etc.), which is defined as:

$$\emptyset_{clay\_KF} = \frac{\emptyset}{1 - f_{inc\_KF}} \tag{3.3.1}$$

$$f_{inc\_KF} = (1 - \emptyset)\frac{\sum_{k=1}^{total\ non-clay} \frac{m_k}{\rho_k}}{\sum_{k=1}^{total\ non-clay} \frac{m_k}{\rho_k} + \sum_{l=1}^{total\ clay} \frac{m_k}{\rho_k}} \tag{3.3.2}$$

Here, f_{inc_KF} is the inclusion (non-clay, NC) volume fraction with respect to non-clay minerals, m is the mass percentage, and ρ is the density (Sierra 2011). This clay phase porosity expression describes how tightly clay polycrystals are packed together in the granular matrix of shale minerals. An important point to note here is only non-clay inclusions and clay minerals are taken into account in equations (3.3.1) and (3.3.2). If the calculation of $\emptyset_{clay\_KF}$ is used for kerogen-rich shale, the contribution of kerogen in shale composition would be temporarily ignored. Moreover, compared to the clay packing density expression in equations (2.3.1) and (2.3.2), a subscript KF (kerogen-free) for $\emptyset_{clay\_KF}$ was added to denote that kerogen is neglected in this calculation for future references.

At first, tensile strength of shale versus KF clay phase porosity, $\emptyset_{clay\_KF}$, was plotted using equations (3.3.1) and (3.3.2) (Figure 3.3.1).

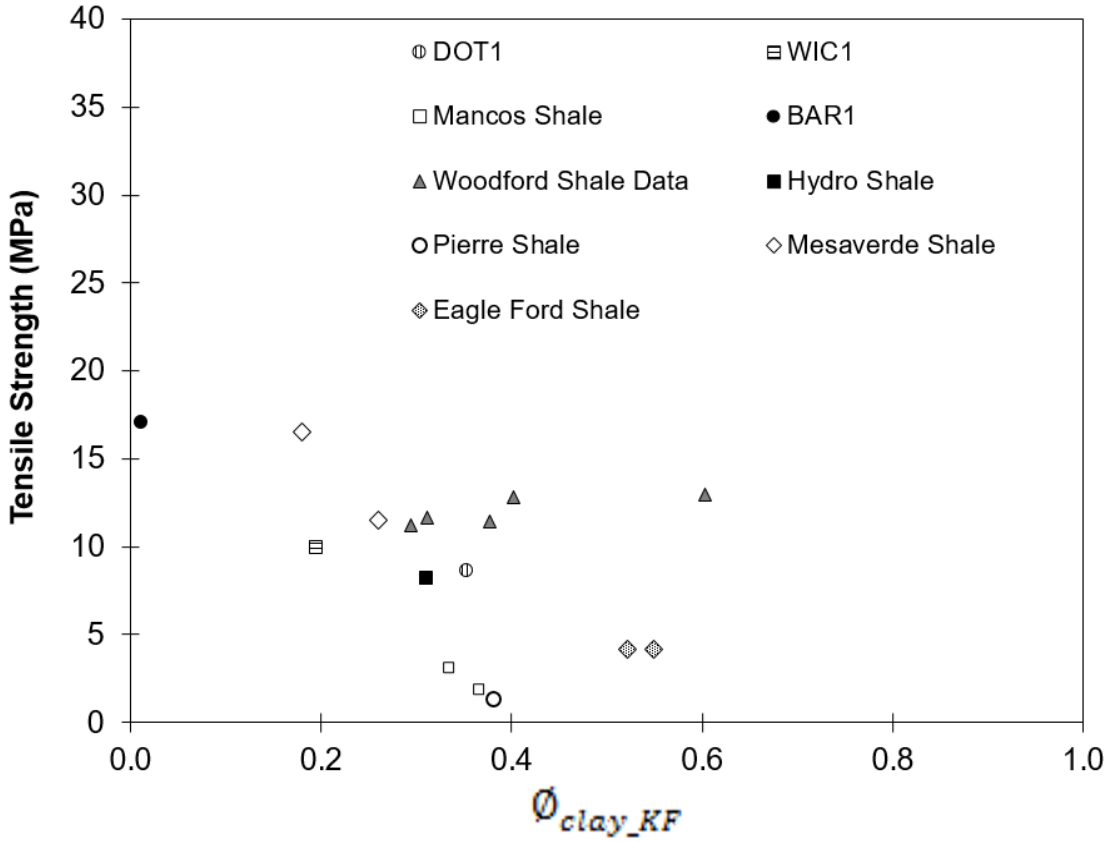

Figure 3.3.1. Tensile strength of some shale versus corresponding $\emptyset_{clay\_KF}$.

As can be seen in Figure 3.3.1, the relationship between tensile strength and KF clay phase porosity, $\emptyset_{clay\_KF}$, is not so pronounced that we barely can apply any linear, power, or polynomial approximations to it. Even though there might exist chances of experimental error for such a small set of data in this model, the link between lateral tensile strength, T_p, and $\emptyset_{clay\_KF}$ is not well defined. The data set in this model includes both kerogen-free shale and kerogen-rich shale. Thus, neglecting kerogen in the calculation of clay phase porosity might not provide a promising modeling result. Saying that, a question arises as to incorporate kerogen into this model.

As introduced at the beginning of this study in some highly mature organic gas shale, since organopores within kerogen are generally isolated bodies, they might be considered to have no connectivity with the mineral matrix (Slatt and O'Brien 2011). As a result, in the model input, matrix-based clay phase porosity acts as the main contributor for tensile behavior in shale. In order to include the kerogen content into the calculation of inclusion volume fraction in kerogen-rich shale, f_{inc_KF} in equations (3.3.1) and (3.3.2) now needs to be slightly modified as:

$$f_{inc\_KR} = (1-\emptyset)\frac{\sum_{k=1}^{total\ non-clay}\frac{m_k}{\rho_k}}{\sum_{k=1}^{total\ non-clay}\frac{m_k}{\rho_k} + \sum_{l=1}^{total\ clay}\frac{m_l}{\rho_l} + \sum_{n=1}^{total\ organic}\frac{m_n}{\rho_n}} \tag{3.3.3}$$

$$\emptyset_{clay\_KR} = \frac{\emptyset}{1-f_{inc\_KR}}. \tag{3.3.4}$$

Figure 3.3.2 shows the results of tensile strength versus KR clay phase porosity, $\emptyset_{clay\_KR}$. Tensile strengths of both kerogen-free shale (Hydro shale, Mesaverde shale, Pierre shale) and the rest of kerogen-rich shale decrease as a function of clay phase porosity. For such a small data set available in this study, the relationship observed in Figure 3.3.2 shows potential for predicting tensile strength from porosity and shale mineral composition. Table 3.3.1 summarizes measured Brazilian indirect tensile strength of all available samples, measured effective porosity using Hg-porosimetry method, converted KR clay phase porosity (included kerogen), and TOC (wt%). All details about the mineralogy of all samples in this model are listed in the appendix.

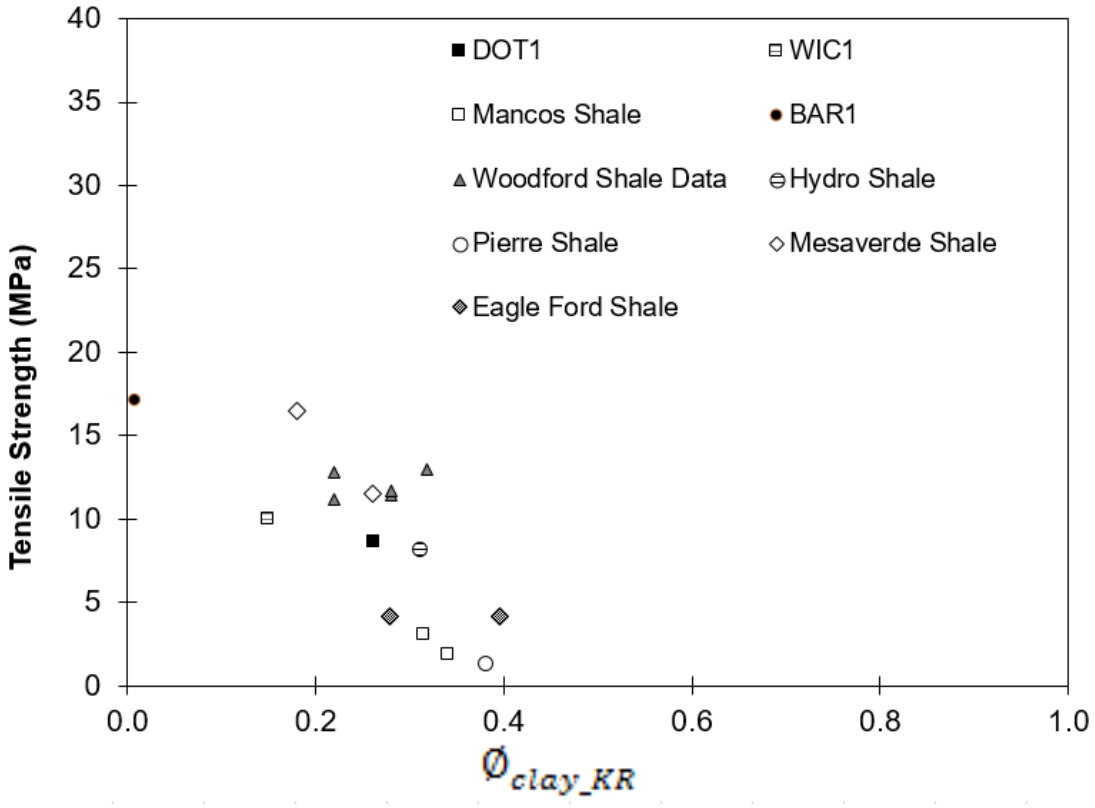

Figure 3.3.2. Tensile strength of selected shale versus $\emptyset_{clay\_KR}$.

Table 3.3.1. Summary of available data with their references for the tensile strength modeling

Sample	Measured Tensile Strength (MPa)	Total porosity	Clay phase porosity (KR)	Wt% of kerogen	Notes
Woodford Shale	13.00	0.146	0.319	18	Sierra et al. (2010)
	12.84	0.104	0.220	18	
	11.44	0.109	0.280	14	
	11.19	0.121	0.220	16	
	11.70	0.185	0.280	18	

Hydro Shale	8.23	0.103	0.310	0	
Pierre Shale	1.36	0.175	0.380	0	
Mesaverde Shale	11.51	0.064	0.260	0	Lin (1983)
	16.52	0.051	0.180	0	
BAR1	17.10	0.006	0.009	13.8	Rybacki et al. (2015)
DOT1	8.70	0.110	0.261	14.9	
WIC1	10.00	0.073	0.150	17	
Eagle Ford Shale	4.18	0.048	0.395	2.1	Lai et al. (2015)
	4.18	0.045	0.278	4.8	
Mancos Shale	1.87	0.060	0.342	0.8	Mokhtari et al. (2014)
	3.08	0.060	0.315	0.8	

3.4 Results and Summary

Available uniaxial tensile strength and porosity data from the studies by Lin (1983), Sierra et al. (2010), Lai et al. (2015), Rybacki et al. (2015), and some of my experimental results were gathered to construct the model. In general, mineralogical compositions were obtained from powder X-ray diffraction, total effective porosities were measured using Hg-injection method or other similar measurements, and ultimate tensile strengths were calculated by conducting standard Brazilian indirect tensile strength tests. First, clay mineral phase plays a dominant role in controlling tensile strength of shale in my hypothesis. I converted total effective porosity into clay phase

porosity, using mineralogical information and equations (3.3.1) and (3.3.2) above. The fact that equations (3.3.1) and (3.3.2) neglect kerogen in the calculation of non-clay inclusion volume fraction of many kerogen-rich shales results in an unclearly-defined relationship between tensile strength and $\emptyset_{clay\_KF}$. Therefore, to accommodate for the lack of kerogen in the previous calculation of f_{inc_KF}, $\emptyset_{clay\_KF}$ is modified slightly to include kerogen content in f_{inc_KR}, as shown in equations (3.3.3) and (3.3.4). The results in Figure 3.3.2 show that as KR clay phase porosity increases, tensile strength of shale decreases. Thus, it is possible to say that tensile strength of organic-rich shale is a function of mineral composition, kerogen content, and porosity:

$$\sigma_{t,KRS} = \mathcal{F}(minerals\ composition, kerogen, \phi). \tag{3.4.1}$$

CHAPTER 4: REFINING THE MODEL

4.1 Percolation Threshold of Clay Phase Porosity at 0.5

Taking a closer look at Figure 2.6.2, most of the experimental data of gypsum and hydroxyapatite range from ϕ =0 - 0.5, which suggests there might exist a percolation threshold of porosity at 0.5. Indeed, going back to the literature, Ortega et al. (2007) confirm that the elastic characteristics of clay phase in shale exhibits a clay packing density percolation threshold of clay packing density $\eta = 0.5$, below which shales lose stiffness or basically have no strength. Figure 4.1.1 describes the elasticity of the porous clay phase as a function of the clay packing density for seven shale samples of different mineralogical composition (Ortega et al. 2007). Here, the elasticity content is represented by an equivalent indentation moduli, M. The indentation stiffness increases with the clay packing density. These stiffness values scale with the clay packing densities almost linearly. Moreover, another interesting fact is that a fitted trend line to those values yields a zero modulus for a clay packing density of a clay-bearing composite of about 0.5. Because the clay packing density $\eta = 1 - \frac{\phi}{1-f_{inc}} = 1 - \emptyset_{clay}$, percolation threshold at clay phase porosity $\emptyset_{clay} = 0.5$ therefore is equally confirmed.

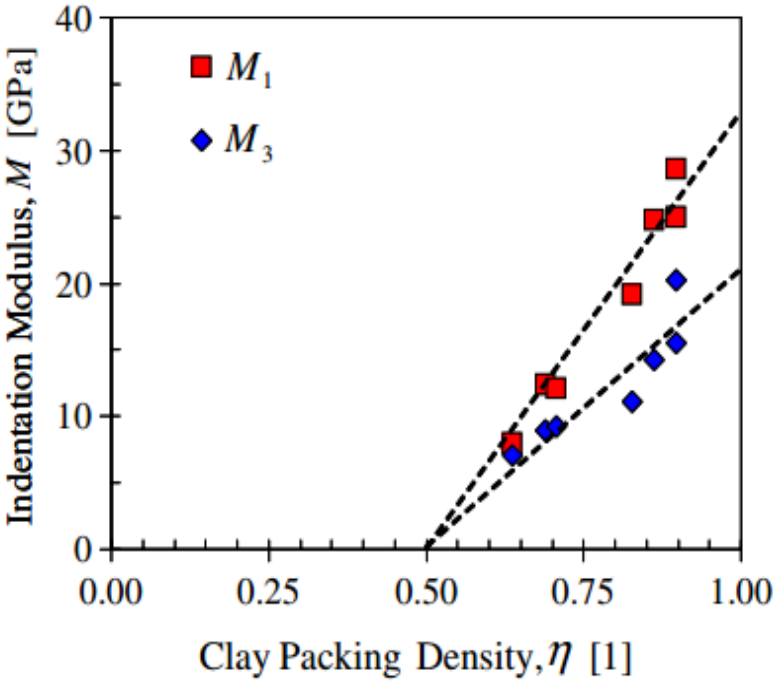

Figure 4.1.1. Porous clay stiffness as indentation modulus M is illustrated as a function of clay packing density of seven shale samples. M_1 represents the elasticity content measured in an indentation test in the direction of the material symmetry (normal to bedding orientation), M_3 (normal to the axis of the material symmetry) (Ortega et al. 2007).

4.2 Verification of Percolation Threshold of Porosity at 0.5 - Introduce New Clay Data

To experimentally verify whether shale has a clay phase porosity threshold at 0.5, a new data set of tensile strength of compacted soils (sand and clay) from a study by Tamrakar et al. (2005) is introduced into our model. In general, these clay-sand mixtures were mixed in the following proportion by weight: 30:70, 35:65, 40:60, 45:55, 50:50, 55:45, 60:40, 65:35, and 70:30. They were mixed thoroughly with distilled water and kept in an air tight plastic bag for a week. The water content was maintained for all

samples at 10%. These samples were then statically compressed by a bellofram cylinder before conducting the tensile strength tests. Dry densities for clay-sand mixture are specified at 1.2 and 1.5 g/cc (Tamrakar et al. 2005). Table 4.2.1 shows that tensile strengths of these compacted soils are significantly small compared to those of shale. This fact is verified in Figure 4.2.1: tensile strengths of the compacted clay-sand mixture can almost be considered to be 0 (MPa).

Table 4.2.1. Data set of compacted soils of sand and clay (Tamrakar et al., 2005). Clay phase porosity is derived using equation (3.3.1) and (3.3.2).

	Tensile strength (MPa)	**Total Porosity**	**Clay phase porosity**
Group 1.5 g/cc	0.005	0.43	0.71
	0.005	0.43	0.71
	0.0063	0.43	0.68
	0.0065	0.43	0.65
	0.0072	0.43	0.62
	0.0076	0.43	0.60
	0.0088	0.43	0.57
	0.0085	0.43	0.55
	0.0098	0.43	0.53
Group 1.2 g/cc	0.0016	0.54	0.80
	0.0018	0.54	0.77
	0.0015	0.54	0.75
	0.0018	0.54	0.73
	0.0019	0.54	0.70
	0.002	0.54	0.68
	0.0023	0.54	0.64

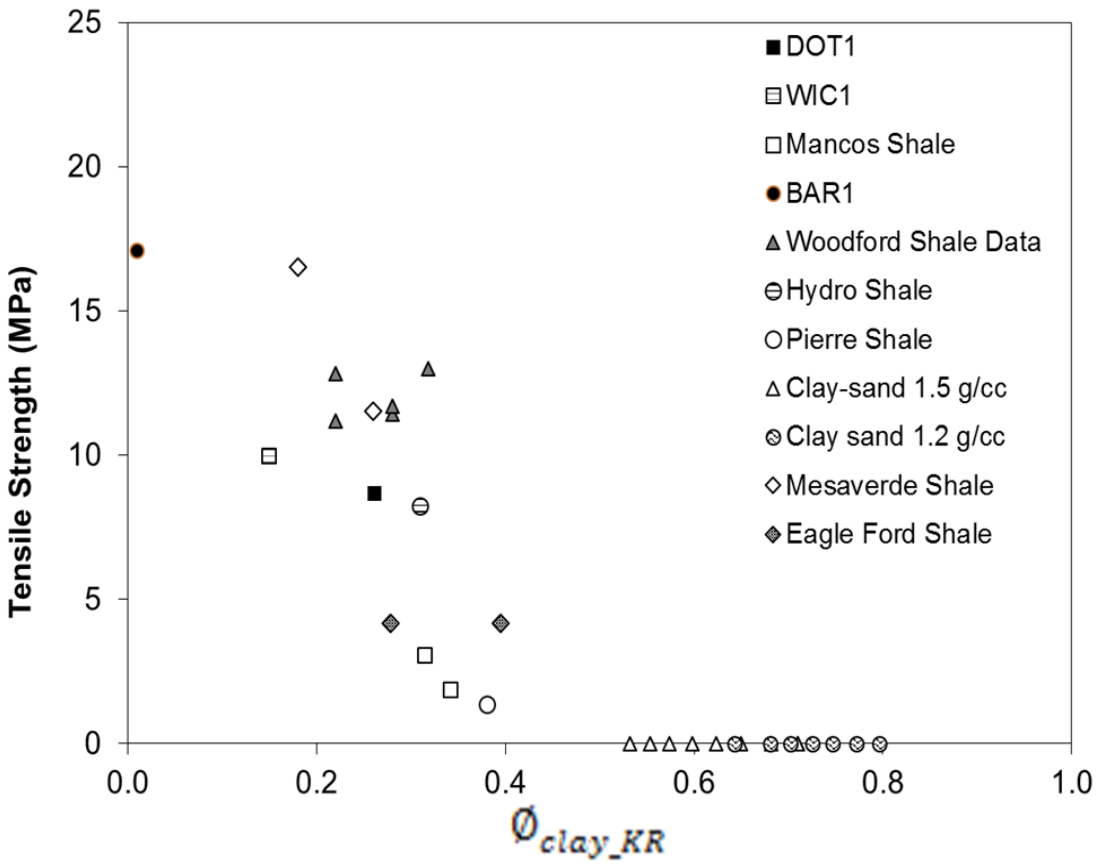

Figure 4.2.1. Tensile strength of some shale versus KR clay phase porosity. Compacted soils of sands and clays are also added into the model to verify the percolation threshold of ϕ_{clay_KR} =0.5.

Applying a clay phase porosity threshold of ϕ_{clay_KR} =0.5 to the model, the power law equation (3) in the Fritsch et al. (2013) model for disk-based porous polycrystals, $\frac{\sum^{ult,t}}{\sigma^{ult,t}} \approx \alpha(1-\phi)^{\beta}$, now can be slightly modified as:

$$\frac{\sum^{ult,t}}{\sigma^{ult,t}} \approx \alpha\left(0.5-\phi_{clay_{KR}}\right)^{\beta}. \tag{4.2.1}$$

Based on equation (4.2.1), as clay phase porosity, ϕ_{clay_KR}, approaches 0, $\sum^{ult,t}$ is basically the tensile strength of solid crystals, $\sigma^{ult,t}$. Therefore, a relationship between α and β is observed in which $\alpha.0.5^{\beta}=1$.

4.3 Ultimate Tensile Strength of Single Homogeneous 'Crystal' of Shale?

In order to estimate ultimate tensile strength, $\sum^{ult,t}$, for any kind of shale based on equation (4.2.1), tensile strength of the solid homogeneous 'crystal' of shale, $\sigma^{ult,t}$, needs to be determined first. This task is an engineering challenge at this time. However, it is possible to set some limits for $\sigma^{ult,t}$. In general, clay minerals are considered to be soft minerals because their Mohs hardness values are usually between 2 to 3. In fact, it is quite difficult to determine their hardness as well as other strength properties due to the microscopic nature of the clay minerals. The Mohs hardness of gypsum and hydroxyapatite are about 2 and 5, respectively. As a result, most clay minerals and mica fall into the hardness ranges for hydroxyapatite and gypsum. Since getting a reasonable value of tensile strength for a solid homogeneous 'crystal' of shale was not possible at this time, I used the uniaxial tensile strength values of single solid crystal of hydroxyapatite (52.2 MPa) and gypsum (17 MPa) that Fritsch et al. (2013) mentioned in their study. Using this approach, the model works reasonably well as can be seen in Figure 4.3.1.

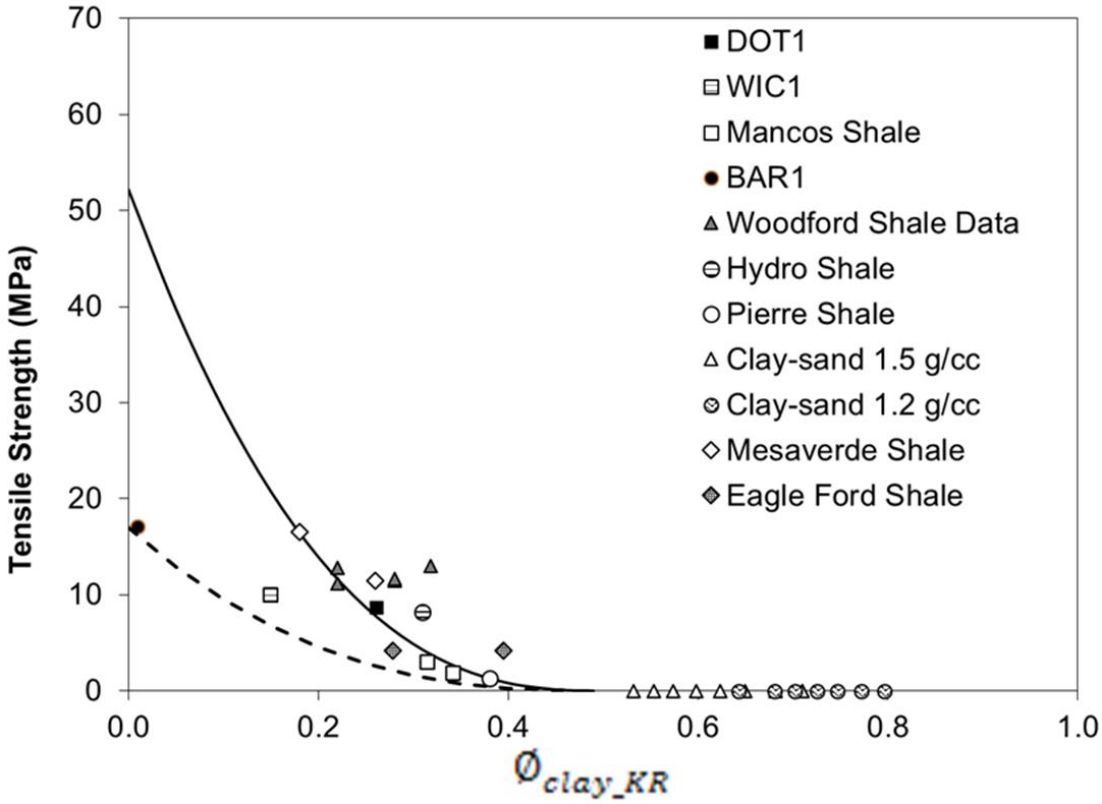

Figure 4.3.1. Tensile strength of some shale as a function of clay phase porosity.

Among the shale data input in this model, the data point of Barnett shale appears to exhibit a low tensile strength value, considering that it has such a low clay phase porosity. This fact might be because Barnett is an overmature gas shale. Thus, porosity in kerogen (organoporosity) is often the dominant type of total porosity development found in these gas shale rocks, whereas other pore types are sparse or absent (Slatt and O'Brien 2011). Not overlooking the potential of kerogen porosity in storage and volumetrics, this study, however, more likely focuses on the pores residing within inorganic matrix of organic-rich shale; those pores are associated more with clay minerals distribution in shale. From this observation, porosity within kerogen might not

count as much in the clay phase porosity input of our model. Therefore, conventional porosity measurements using well logs or common Hg-injection method in most laboratories works just fine for the scope of this study. It is possible that the model might not be applicable for every kind of shale; especially for overmature and mature gas shale. However, if using conventional porosity measurements as stated above, this model works reasonably well for immature and mature oil shale (i.e., Woodford shale). Since the mercury injection porosimetry method does not capture micropores and nanopores (<2nm), which may be abundant in highly mature shale and partially stay within the organic compounds, other kinds of porosity measurements for overmature shale might be needed to obtain better input for the model. Otherwise, other factors regardless of clay phase porosity should be taken into consideration when estimating tensile strength of these rocks.

4.4 Fracture Toughness Estimation from Clay-phase Porosity

Fracture toughness (K_{IC}) of a rock represents the ability to resist fracture propagation from preexisting cracks under Mode-I (opening) condition. It is an important parameter in theoretical studies and engineering applications such as hydraulic fracturing design. Due to the complexity of the three-point bending fracture tests in terms of sample preparation, there are not many experimental measurements of fracture toughness reported for shale in the literature (Wang et al. 2007). Moreover, many laboratory testing methods have been proposed to measure fracture toughness; however; all of them are considerably complicated and more costly than other rock mechanics tests (Wang et al. 2007; Zhang 2002). A simple method estimating fracture toughness of rock, therefore, would be significantly helpful.

Many empirical relationships have been reported in the literature between Mode-I fracture toughness and physical-mechanical properties of rock, such as Young's modulus, Poisson's ratio, hardness, grain size, tensile strength, uniaxial compressive strength, and velocity of primary acoustic wave (Brown and Reddish 1997; Al-Shayea et al. 2000; Zhang 2002, Backers 2005; Nasseri and Mohanty 2008). The question is: "Which relation appears to be reliable and consistent enough for such a heterogeneous family like shale?" In order to answer that question, I used the Woodford shale data set in the study by Sierra et al. (2010) to do a simple check and verify the accuracy of some of these correlations. Even though the Woodford shale data set in the study by Sierra et al. (2010) does not incorporate every single parameter mentioned previously, I attempted to derive some statistical correlations between Mode-I fracture toughness and tensile strength, Young's modulus, acoustic compressional wave velocity, and bulk density, respectively. The comparison results are summarized in Table 4.4.1 and are illustrated in Figure 4.4.1 and Figure 4.4.2.

Table 4.4.1. Summary of four correlations of fracture toughness with tensile strength, Young's modulus, compression wave velocity, and bulk density. K_{IC} is Mode-I fracture toughness, MPa·m$^{0.5}$; σ_t is tensile strength, MPa; E is Young's modulus, GPa; V_p is compressional sonic velocity, km/s. Data was taken from Sierra et al. 2010.

	Correlations with fracture toughness	R^2
Tensile Strength	$\sigma_t = 2.8761\ K_{IC} + 9.4003$	0.9297
Bulk density	$\rho = -0.2888\ K_{IC} + 2.443$	0.8321
Young's Modulus	$E = -2.498\ K_{IC} + 22.303$	0.2299
Compressional wave velocity	$V_p = 0.0156\ K_{IC} + 3.3795$	0.0016

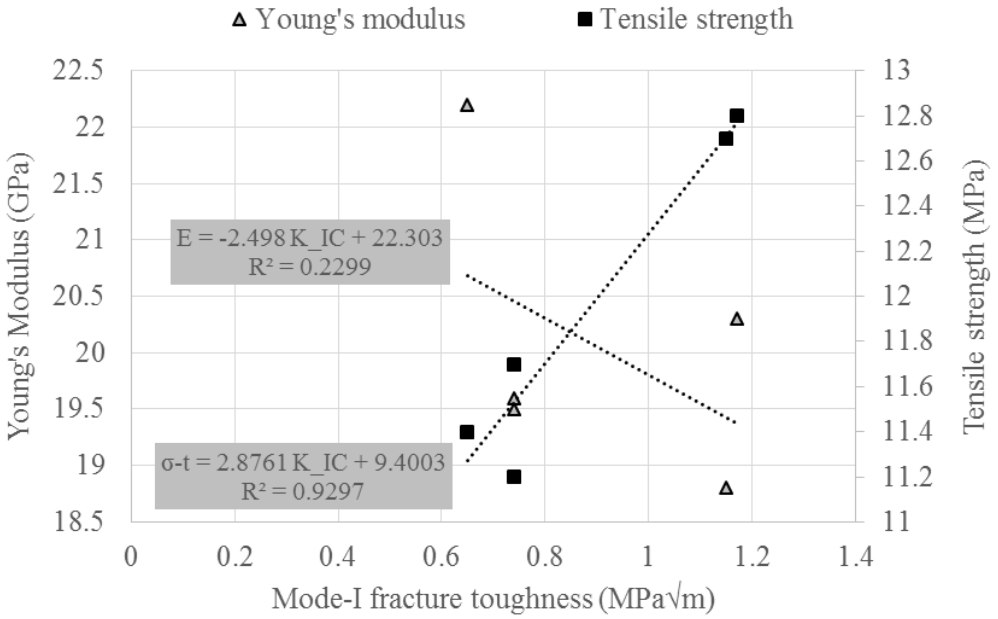

Figure 4.4.1. Correlation between Mode-I fracture toughness, K_{IC}, with Young's modulus, *E*, and tensile strength, σ_t (data was taken from Sierra et al. 2010).

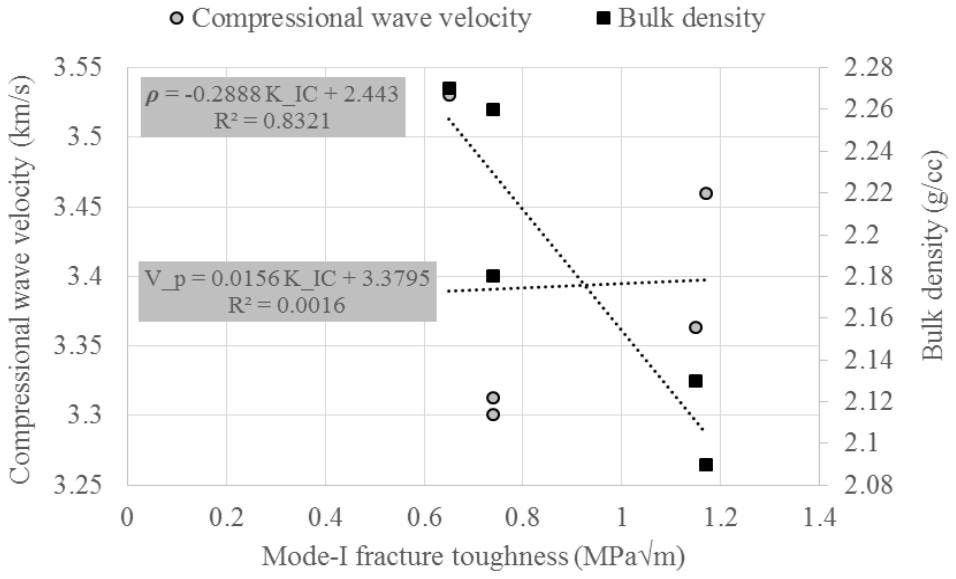

Figure 4.4.2. Correlation between Mode-I fracture toughness, K_{IC}, with compressional wave velocity, V_p, and bulk density, ρ (data was taken from Sierra et al. 2010).

The first two correlations between Mode-I fracture toughness with tensile strength and bulk density in Table 4.4.1 show significantly high values of R^2 (>0.8). On top of that, for such a small data set of Woodford shale, the relationship between Mode-I fracture toughness and tensile strength is significantly pronounced (R^2 ~ 0.93). On the other hand, the correlations with V_p and E seem to be not reliable because of the low values of R^2. Indeed, to improve the accuracy of these fracture toughness correlations, experimental data from many other kinds of shale is needed. It is also a good routine to double check the derivations from logging data versus those derived from values measured on cores. However, considering that the empirical linear relationship between Mode-I fracture toughness and tensile strength in the Woodford shale data set shows great potential to derive fracture toughness, I collected more experimental data from the literature to expand the relationship for more types of rocks. Tensile strength and fracture toughness data of many types of rocks such as oil shale, siltstone, and sandstone collected from a study by Zhang (2002) are shown in Figure 4.4.3. Zhang (2002) also proposed an empirical relation between Mode-I fracture toughness and tensile strength as:

$$K_{IC\ (Zhang\ 2002)} = 0.1453\sigma_t \text{ with } r^2=0.94. \quad (4.4.1)$$

.

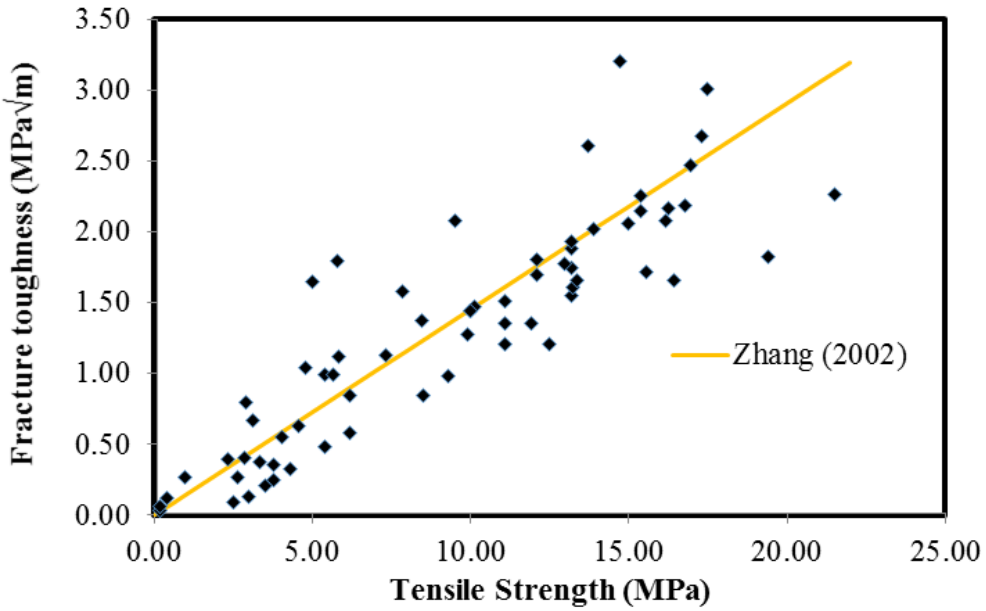

Figure 0.4.3. K_{IC} versus σ_t of rocks (data was taken from Zhang 2002).

Many other empirical relations between Mode-I fracture toughness and tensile strength are available in the literature. The difference in the proportionality coefficient and the coefficient of determination of these empirical relations is probably due to different testing methods and various rock types included in the studies (Wang et al. 2007). Using the correlation in the study by Zhang (2002), an estimation of fracture toughness from clay-phase porosity can be summarized as

$$K_{IC} \approx 0.1453\, \sigma^{\mathrm{ult,t}}\, \alpha(0.5-\phi)^{\beta} \tag{4.4.2}$$

where $0.5^{\beta}\alpha = 1$, $\sigma^{\mathrm{ult,t}}$ is the uniaxial tensile strength values of single solid crystal of hydroxyapatite (52.2 MPa) or gypsum (17 MPa) (Fritsch et al. 2013) that constrains the upper and lower bounds, respectively, for the model.

As the Woodford shale data taken from a study by Sierra et al. (2010) are well-fitted in the constrained boundaries (Figure 4.4.3), this model works reasonably well for

this organic-rich shale. Due to the limited resources of experimental measurements on fracture toughness of shale, only the Woodford shale data set is available for the verification of the fracture toughness model. As a result, in order to narrow the range of fracture toughness for those shales which have a low clay phase porosity, more experimental measurements of different types of shale in this topic are indeed necessary.

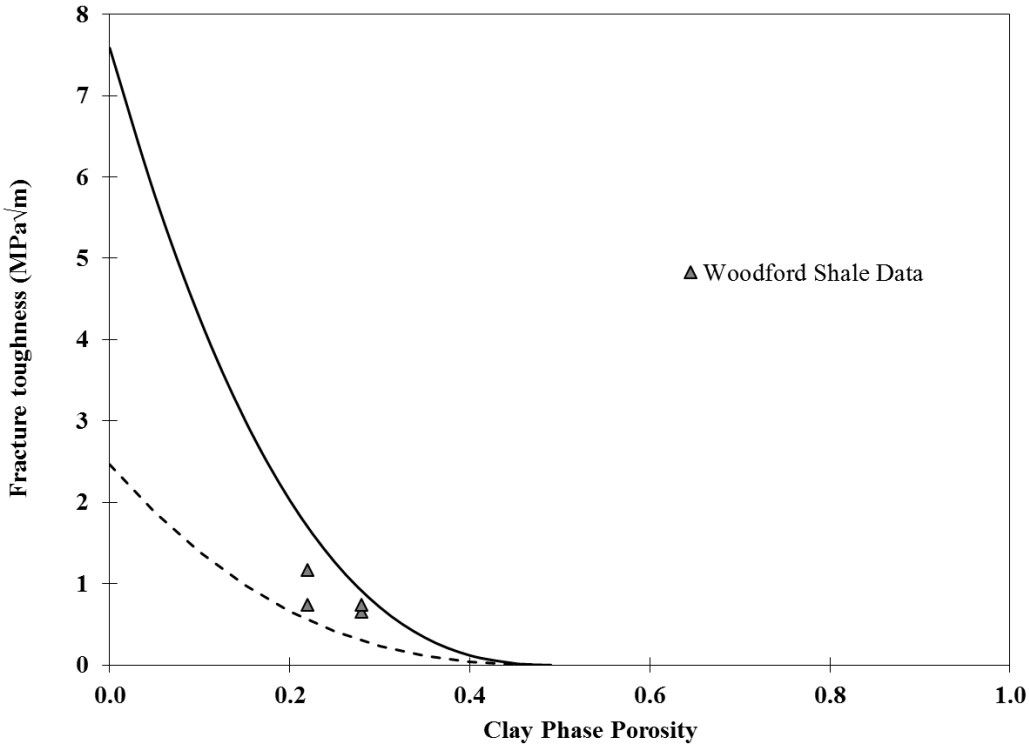

Figure 4.4.3. Fracture toughness as a function of clay phase porosity.

4.5 Discussion

For organic-free shale, the model proves that the granular nature of clays and non-clay minerals primarily controls tensile strength of these rocks. The fact that the model shows a well-defined decreasing trend in tensile strength as clay phase porosity

increases means that the model is flexible to be applied for many kinds of organic-free shale, regardless of their mineralogical composition and porosity or multi-porosity nature.

On the other hand, for organic-rich shale, the kerogen content was incorporated into the model by modifying the original calculation of clay phase porosity of kerogen-free shale. A decreasing trend in tensile strength was also observed as the modified clay phase porosity increases. To some extent, given that the model only needs mineralogy information, kerogen content, and porosity as primary input for tensile strength estimation, it almost fulfills the hope to simplify the polymer nature of kerogen observed in organic-rich shale, yet absent in organic-free shale. The granular and polymer nature of organic-rich shale appears to be complex, yet it looks questionably simple in the model of this study.

Taking a step back and revisiting the micro-beam testing mentioned in Section 2.5, it was discovered that the polymer tensile nature of kerogen would be underestimated if quantifying kerogen by its content only. Granular materials like clays and non-clay minerals behave elastically, yet they are still brittle components. In contrast, kerogen, which is woven within shale mineral matrix, is a polymer-like material. Recalling from micro-beam testing in Figure 2.5.2, the polymer-like string of kerogen keeps the beam attached to the support after a total tensile failure of the micro-beam T_1 and is responsible for the micro-beam displacement recovery. Among the four loading/displacement curves plotted in figure 4.5.1 of four tested micro-beam in the study by Abousleiman et al. (2016), T_1 and T_2 show strain-softening and strain-

hardening behavior, respectively, before ductile/plastic failures, whereas T_3 and T_4 possess brittle failure with little or no yield.

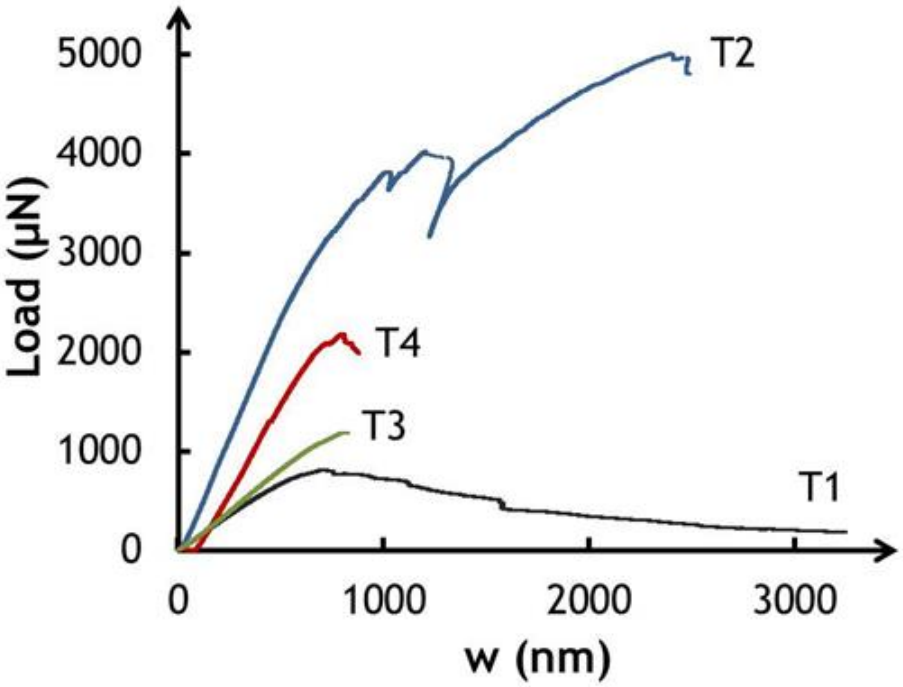

Figure 4.5.1. Loading/displacement curves of four tested micro-beam in the study by Abousleiman et al. (2016).

As evident in figure 4.5.1, micro-beam T_1 and T_2 experienced complex strain-softening and strain-hardening post-yield behavior, respectively, while T_3 and T_4 clearly show brittle failure modes. The ultimate tensile load of the micro-beams shown in figure 4.5.1 is in fact equivalent to unconfined tensile strength, UTS, which is also the interest of this study. Classical techniques measured tensile strength of rocks (i.e., Brazilian indirect tensile strength test) might provide reasonable UTS measurements for kerogen-free shale. However, the UTS observed in kerogen-rich shale might be much more complex, as proved in figure 4.5.1. Mode-I crack opening in hydraulic fracturing,

as a result, occurs in a complex "composite polymer-type weaved porous material" while the mechanics still remains unknown (Abousleiman et al. 2016).

To understand why the ultimate tensile strength in kerogen-rich shale should not be treated as a simple indirect tensile strength measurement, the modulus of toughness of kerogen-bearing shale, defined as the work/energy needed before the total rupture, was illustrated in figure 4.5.2. Even though micro-beam T_3 requires a higher load to be fractured than T_1, it only requires about 10% of the toughness needed to break T_1. As a result, the kerogen effect on the modulus of toughness and/or the tensile strength is much larger than the anisotropy effect ever observed in classical tensile strength testing protocols. For that reason, mineralogy information and porosity are only enough to quantify the granular nature, but not the polymer woven into the clay and non-clay matrices behavior as was recently observed in kerogen-rich shale experiments. It was suggested that this model, as well as other existing models using empirical equations to predict tensile strength of organic-rich shale, might not be perfect to be a composite model for KRS in general. As a result, future improvements are indeed necessary.

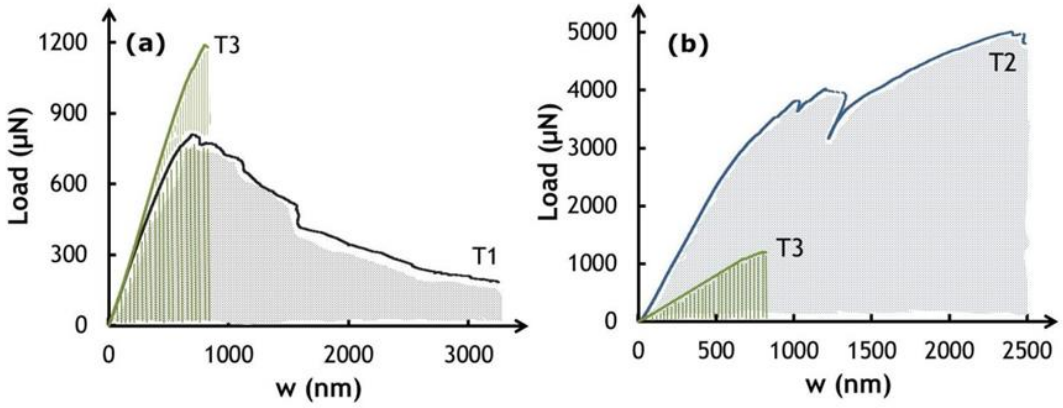

Figure 4.5.2. Moduli of toughness of 'granular shale' micro-beam T_3 when compared to the 'granular and polymer shale' micro-beams T_1 and T_2. The two

shaded areas where T_3 required about 10-15% of the toughness needed to break T_1 and T_2, respectively (Abousleiman et al. 2016).

Last but not least, the complex polymer nature of kerogen-rich shale can be imagined in a simple way illustrated in Figure 4.5.1. Once initiated, tensile fracture can easily propagate all the way through the brittle, granular shale matrix of clays and non-clay minerals. However, as soon as the tensile fracture propagates and its tip hits the kerogen, the fracture deteriorates and fracturing process stops. The energy required to break the brittle minerals matrix is sufficiently not enough to break the polymer-quality kerogen, which means higher energy is needed to prevent the process of hydraulic fracturing from stopping. This is what most tensile crackings in kerogen-rich shale formations experienced in the field and why hydraulic fracturing is a multi-phase process. The answer is, again, the polymer nature of kerogen interwoven in the minerals matrix of kerogen-rich shale.

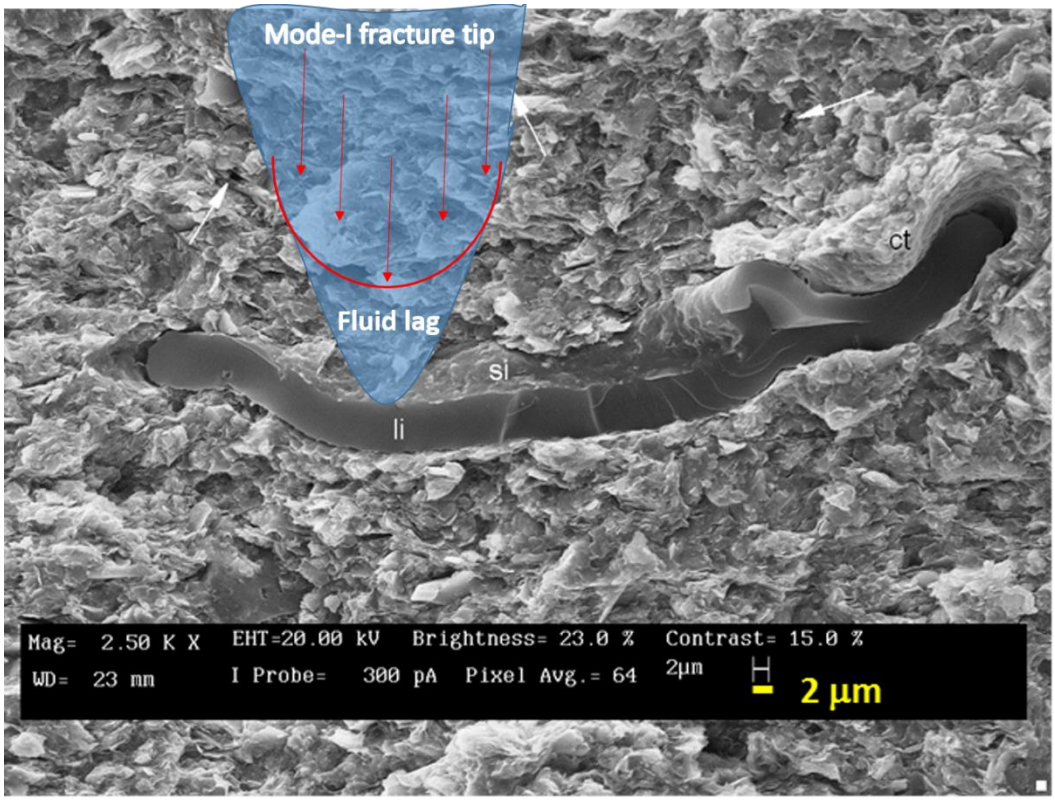

Figure 4.5.3. A simple illustration of the tip of Mode-I fracture deteriorated in hydraulic fracturing due to the presence of kerogen in kerogen-rich shale (modified from Abousleiman et al. 2016).

4.6 Conclusions

- The composite nature of kerogen-rich shale tensile failure is a complex system of both heterogeneous porous sediments and polymer quality kerogen. This study isolates the part of porosity residing within kerogen (organoporosity) and mostly concentrates on the contribution of KR clay phase porosity, ϕ_{clay_KR}, on controlling shale tensile strength. This clay phase porosity incorporates the kerogen content in organic-rich shale to accommodate for the lack of kerogen in the old calculation of clay phase porosity, which was originally proposed in kerogen-free shale in a study by Ortega et al. (2007). Experimental results

showed that tensile strength of shale acts as a power law function of KR clay phase porosity in which $\frac{\sum^{ult,t}}{\sigma^{ult,t}} \approx \alpha(0.5 - \phi_{clay\_KR})^{\beta}$ with $0.5^{\beta}\alpha = 1$.

- Due to the microscopic nature of clay minerals, obtaining a measurement of tensile strength of a single solid homogeneous 'crystal' of shale, $\sigma^{ult,t}$, appears to be impossible at this time. However, if using uniaxial tensile strength of solid crystal, $\sigma^{ult,t}$, of gypsum and hydroxyapatite, respectively, as the lower and upper constraints, the model works reasonably well for many immature and mature oil shales. Moreover, conventional porosity measurements using well logs or the common mercury injection porosimetry method in most laboratories work fine for the scope of this study. Therefore, time and expense demand for laboratory testing are certainly minimized.
- Experimentally, Mode-I fracture toughness of rocks scales linearly with tensile strength. As a result, fracture toughness can be roughly estimated as well using the approach in this study. The correlation of Mode-I fracture toughness with KR clay phase porosity is written as $K_{IC} \approx 0.1453\ \sigma^{ult,t}\ \alpha\left(0.5 - \phi_{clay_{KR}}\right)^{\beta}$. Measured Mode-I fracture toughness of organic-rich Woodford Shale is well-fitted in the constrained boundaries of this model.
- For organic-free shale, the model proves that the granular nature of clays and non-clay minerals primarily controls tensile strength of these rocks; thus, the model is flexible to be applied for many kinds of shale, regardless of their mineralogical composition and porosity or multi-porosity nature. On the other hand, for organic-rich shale, the kerogen content was incorporated into the model to accommodate the lack of kerogen in the original calculation of clay

phase porosity of kerogen-free shale. To some extent, this tensile strength model has simplified the complex granular and polymer nature of kerogen-rich shale and almost clears the gap - the polymer behavior of kerogen - between organic-rich shale and organic-free shale. However, the modulus of toughness of kerogen-rich shale, defined as the work/energy needed before the total rupture, proves that the energy required to break that composite polymer-bearing material is significantly higher than that of kerogen-free shale. As a result, the kerogen effect on the modulus of toughness and/or the tensile strength is much larger than the anisotropy effect ever observed in classical tensile strength studies. Meaning that, mineralogy information and porosity are only enough to quantify the granular nature, but not the polymer woven into the clay and non-clay minerals matrix in kerogen-rich shale. As a result, this model as well as other existing models using empirical equations to predict ultimate tensile strength might not be perfect to be a composite model for organic-rich shale in general. Future improvements are indeed necessary.

REFERENCES

Abousleiman, Y., Hull, K., Han, Y., Al-Muntasheri, G., Hosemann, P., Parker, S., and Howard, C.B. 2016. The Granular and Polymer Nature of Kerogen Rich Shale. *Acta Geotechnica*. http://dx.doi.org/10.1007/s11440-016-0435-y

Abousleiman, Y., Tran, M., Hoang, S., Bobko, C., Ortega, J. A., and Ulm, F.-J. 2007. Geomechanics Field and Laboratory Characterization of Woodford Shale: The Next Gas Play. Presented at the SPE Annual Technical Conference and Exhibition, Anaheim, California, 11-14 November. SPE-110120-MS. http://dx.doi.org/10.2118/110120-MS.

Abousleiman, Y., Tran, M. H., Hoang, S., Ortega, J. A., and Ulm, F.-J. 2009. GeoMechanics Field Characterization of the Two Prolific U.S. Mid-West Gas Plays with Advanced Wire-Line Logging Tools. Presented at the SPE Annual Technical Conference and Exhibition, New Orleans, Louisiana, 4-7 October. SPE-124428-MS. http://dx.doi.org/10.2118/124428-MS.

Al-Shayea, N., Khan, K., Abduljauwad, S. 2000. Effects of Confining Pressure and Temperature on Mixed-Mode (I–II) Fracture Toughness of a Limestone Rock. *International Journal of Rock Mechanics and Mining Sciences* **37** (4): 629-643.

Backers, T. 2005. *Fracture Toughness Determination and Micromechanics of Rock under Mode I and Mode II Loading*. Dissertation, University of Potsdam, Potsdam, Germany.

Brown, G. J. and Reddish, D. J. 1997. Experimental Relations between Rock Fracture Toughness and Density. *International Journal of Rock Mechanics and Mining Sciences* **34** (1):153-155.

Fritsch, A., Hellmich, C., and Young, P. 2013. Micromechanics-Derived Scaling Relations for Poroelasticity and Strength of Brittle Porous Polycrystals. *Journal of Applied Mechanics* **80** (2). http://dx.doi.org/10.1115/1.4007922.

Gale, J. F. W., Reed, R. M., and Holder, J. 2007. Natural Fractures in the Barnett Shale and Their Importance for Hydraulic Fracture Treatments. *AAPG Bulletin* **91**: 603–622 http://dx.doi.org/10.1306/11010606061.

Griffith, A. A. 1921. The Phenomena of Rupture and Flow in Solids, Philosophical transactions of the royal society of London, Series A **221**: 163-198.

Lai, B. T., Li, H., Liu, H. H., Zhang, J. L., and Georgi, D. 2015. Brazilian Tensile Strength Test of Organic-rich Shale. Presented at the Abu Dhabi International Petroleum Exhibition and Conference, Abu Dhabi, UAE, 9-12 November. SPE-177644-MS. http://dx.doi.org/10.2118/177644-MS.

Lin, W. 1983. Mechanical Properties of Mesaverde Sandstone and Shale at High Pressures. Lawrence Livermore National Laboratory.

Mokhtari, M., Bui, B.T. and Tutuncu, A.N. 2014. Tensile Failure of Shale: Impacts of Layering and Natural Fractures. Presented at the SPE Western North American and Rocky Mountain Joint Regional Meeting, Denver, Colorado, 6–18 April. SPE-169520-MS.

Nasseri, M. and Mohanty, B. 2008. Fracture Toughness Anisotropy in Granitic Rocks, *International Journal of Rock Mechanics and Mining Sciences* **45** (2): 167-193. http://dx.doi.org/10.1016/j.ijrmms.2007.04.005.

Nasseri, M., Mohanty, B., Robin, P.-Y.F. 2005. Characterization of Microstructures and Fracture Toughness in Five Granitic Rocks. *International Journal of Rock Mechanics & Mining Sciences* **42**: 450–460. http://dx.doi.org/10.1016/j.ijrmms.2004.11.007.

Ortega, A. J., Ulm, F.-J., and Abousleiman, Y. 2007. The Effect of Nanogranular Nature of Shale on Their Poroelastic Behavior. *Acta Geotech* **2**: 155–182. http://dx.doi.org/10.1007/s11440-007-0038-8.

Ortega, A. J., Ulm, F.-J., and Abousleiman, Y. 2009. The Nanogranular Acoustic Signature of Shale. *Geophysics* **74** (3):65–84. http://dx.doi.org/10.1190/1.3097887.

PetroTech Associates. 2014. Clay SEM Images (14 October 2014 revision), http://www.petrotech-assoc.com/prod01.htm. (Accessed 20 October 2015).

Ratigan, J. L. 1982. An Examination of the Tensile Strength Of Brittle Rock. Presented at the 23rd U.S Symposium on Rock Mechanics (USRMS), Berkeley, California, 25-27 August. ARMA-82-421.

Rybacki, E., Reinicke, A., Meier, T., Makasi, M., and Dresen, G. 2015. What Controls The Mechanical Properties of Shale Rocks? – Part I: Strength and Young's modulus. *Journal of Petroleum Science and Engineering* **135**: 702-722.

Sierra, R. 2011. *Integrated Geomechanics and Geological Characterization of the Devonian-Mississippian Woodford Shale.* MS thesis, University Of Oklahoma, Norman, OK.

Sierra, R., Tran, M. H., Abousleiman, Y. N., and Slatt, R. M. 2010. Woodford Shale Mechanical Properties and the Impacts of Lithofacies. Presented at the 44th US Rock mechanics Symposium and 5th USCanada Rock Mechanics Symposium, Salt Lake City, Utah, USA, 27-30 June. ARMA-10-461.

Slatt, R. M. and Abousleiman, Y. 2011. Merging Sequence Stratigraphy and Geomechanics for Unconventional Gas Shales. *The Leading Edge* **30**: 274–282. http://dx.doi.org/10 546.1190/1.3567258.

Slatt, R. M., Buckner, N., Abousleiman, Y., Sierra, R., Philp, P. R., Miceli-Romero, A., Portas, R., O'Brien, N., Tran, M., Davis, R., and Wawrzyniec, T. 2012. Outcrop-Behind Outcrop (Quarry), Multiscale Characterization of the Woodford Gas Shale,

Oklahoma. *J. Breyer, ed., Shale reservoirs — Giant resources for the 21st century: AAPG Memoir* **97**: 382–402.

Slatt, R. M., and O'Brien N. R. 2011. Pore Types in the Barnett and Woodford Gas Shale: Contribution to Understanding as Storage and Migration Pathways in Fine-grained Rocks. *AAPG Bulletin* **95** (12): 2017-2030.

Tamrakar, S. B., Toyosawa, Y., Mitachi, T., and Itoh, K. 2005. Tensile Strength of Compacted and Natural Soils Using Newly Developed Tensile Strength Measuring Apparatus. *Soils and Foundations* **45** (6):103-110.

Tran, M. H. 2009. *Geomechanics Field and Laboratory Characterization of the Woodford Shale.* MS thesis, University of Oklahoma, Norman, OK.

Ulm, F.-J. and Abousleiman, Y. 2006. The Nanogranular Nature of Shale. *Acta Geotechnica* **1** (2): 77–88. http://dx.doi.org/10.1007/s11440-006-0009-5.

Vernik, L. and Nur, A. 1992. Ultrasounic Velocity and Anisotropy of Hydrocarbon Source Rocks. *Geophysics* **57** (5): 727–735. http://dx.doi.org/10.1190/1.1443286.

Wang, J., Zhu, J., Chiu, C., and Zhang, H. 2007. Experimental Study on Fracture Toughness and Tensile Strength of a Clay. *Engineering Geology* **94**: 5-75 http://dx.doi.org/10.1016/j.enggeo.2007.06.005

Zeszotarski, J. C., Chromik, R. R., Vinci, R. P., Messmer, M. C., Michels, R., and Larsen, J. W. 2004. Imaging and Mechanical Property Measurements of Kerogen via Nanoindentation. Geochimica et Cosmochimica Acta 68 (20): 4113–4119. http://dx.doi.org/10.1016/j.gca.2003.11.031.

Zhang, Z.X. 2002. An empirical relation between mode I fracture toughness and the tensile strength of rock. *International Journal of Rock Mechanics and Mining Sciences* **39**: 401-406.

APPENDIX: MINERALOGY INFORMATION

Sample	Measured Tensile (MPa)	Total porosity	Qtz	Ksp	Plag	Cal	Dol	Ank	Anh	Siderite	Pyr	Clay	Kerogen
WF1	13	0.146	53	2	1	1	0	2	0	0	3	20	18
WF2	12.84	0.104	53	2	1	1	0	2	0	0	3	20	18
WF4	11.435	0.109	2	2	0.5	0.5	4	16	0	0	2	25	14
WF5	11.1934	0.121	2	2	0	0	0	7	0	0	7	30	16
WF6	11.6955	0.185	2	3	0	0	1	2	0	0	6	31	18
Hydro	8.23	0.103	62	0	6	0	0	0	0	0	2	31	0
Pierre	1.36	0.175	23	12	7	0	13	0	0	5	4	36	0
Mesaverde	11.51	0.064	75	0	5	0	0	0	0	0	0	20	0
Shale	16.52	0.051	65	0	0	5	5	0	0	0	0	25	0
BAR1	17.1	0.006	21.5	6.2	0	5.2	0	0	0	0	0.7	52.1	13.8
DOT1	8.7	0.11	12.7	0	0	41.6	0	0	0	0	1.8	18	14.9
WIC1	10	0.073	13.2	1.6	0	33.9	0	0	0	0	2.2	25.6	17
Eagle	4.18	0.048	21.2	0	0	68	2.3	0	1.9	0	0.3	4.2	2.1

Ford Shale	4.18	0.045	25.1	0	0	62.6	1	0	2.1	0	0.2	4.3	4.8
Mancos Shale	1.87	0.06	52.9	3.7	5.8	9.1	15.6	0	0	0	0.7	11.3	0.8
	3.08	0.06	60	2.3	2.2	11.8	9.1	0	0	0	0.8	13	0.8